Pure Hydrolysis of Polyamides: A Comparative Study

Brette, Mathis Mortensen; Holm, Allan Hjarbæk; Drozdov, Aleksey D.; Christiansen, Jesper de Claville

Published in:
Chemistry

DOI (link to publication from Publisher):
10.3390/chemistry6010002

Publication date:
2024

Document Version
Publisher's PDF, also known as Version of record

chemistry

MDPI

Review

Pure Hydrolysis of Polyamides: A Comparative Study

Mathis Mortensen Brette [1], Allan Hjarbæk Holm [2], Aleksey D. Drozdov [1] and Jesper de Claville Christiansen [1,*]

[1] Department of Materials and Production, Aalborg University, Fibigerstræde 16, 9220 Aalborg, Denmark; m.brettemortensen@outlook.com (M.M.B.); aleksey@mp.aau.dk (A.D.D.)
[2] Grundfos A/S (Danske Salgsselskab), Martin Bachs Vej 3, 8850 Bjerringbro, Denmark; aholm@grundfos.com
* Correspondence: jc@mp.aau.dk

Abstract: Polyamides (PAs) undergo local environmental degradation, leading to a decline in their mechanical properties over time. PAs can experience various forms of degradation, such as thermal degradation, oxidation, hydrothermal oxidation, UV oxidation, and hydrolysis. In order to better comprehend the degradation process of PAs, it is crucial to understand each of these degradation mechanisms individually. While this review focuses on hydrolysis, the data from degrading similar PAs under pure thermal oxidation and/or hydrothermal oxidation are also collected to grasp more perspective. This review analyzes the available characterization data and evaluates the changes in molecular weight, crystallinity, chemical structure, and mechanical properties of PAs that have aged in oxygen-free water at high temperatures. The molecular weight and mechanical strength decrease as the crystallinity ratio rises over aging time. This development is occurring at a slower rate than degradation in pure thermal oxidation. By combining the data for the changes in mechanical properties with the ones for molecular weight and crystallinity, the point of embrittlement can be not only predicted, but also modeled. This prediction is also shown to be dependent on the fibers, additives, types of PA, pH, and more.

Keywords: hydrolysis; polyamide; aging; degradation; crystallization; embrittlement

Citation: Brette, M.M.; Holm, A.H.; Drozdov, A.D.; Christiansen, J.d.C. Pure Hydrolysis of Polyamides: A Comparative Study. *Chemistry* **2024**, *6*, 13–50. https://doi.org/10.3390/chemistry6010002

Academic Editors: Lorentz Jäntschi and Dusanka Janezic

Received: 13 September 2023
Revised: 27 November 2023
Accepted: 28 November 2023
Published: 20 December 2023

1. Introduction

Polyamides (PAs) are thermoplastic polymers thriving as household and engineering materials because of their high elasticity, mechanical strength, high melting point, chemical resistance to oil, and barrier properties against liquids and gases. These properties make them adequate not only as carpets, stockings, and clothing as fibers but also gears, pipelines, and automotive components as plastics. In society, they are commonly referred to as nylon [1–4]. In their applications, PAs are exposed to chemical aging, which negatively impacts their mechanical properties in the long term. When in contact with water or humidity for a long period of time, PAs can undergo hydrolysis. This causes a cut within the polymer chains, leading to a decrease in molecular weight over time [5,6].

While the degradation mechanism of PAs in water is seemingly straightforward from a chemical point of a view, when diving deeper,it can be found that a complex coupling of mechanisms occurs. Water reacts with the amide group and induces chain scission. This is the reverse polymerization reaction from the condensation of the acid and amine monomers. The presence of oxygen both in the air and dissolved in the aqueous solution is of great importance. This oxygen oxidizes the polymer, which not only further degrades it, but also introduces a whole new set of different chemical degradation pathways. Thermal oxidation starts with the abstraction of a hydrogen at the aliphatic carbon chain by oxygen radicals. The carbon atoms adjacent to the amide group turn become radical from the homolytic cleavage of their hydrogen [5,7–10]. This further leads the material to experience yellowing, discoloration, cross-linking, embrittlement, and so on. The thermal oxidation of PAs has been investigated in many articles over the years [9,11–19].

To this day, several reviews have been published concerning the degradation of PAs. In 1998, Thanki et al. [20] published a literature review on the thermal oxidation and photooxidation of PA66. A couple of years later, Shamey et al. [5] reviewed the types of degradation, the factors impacting them, and their means of characterization for PA66 in 2003. Finally, Venoor et al. [21] reviewed the physical and chemical interactions between PAs and water in 2020. In this review, the authors centered their attention on the transport of moisture within the polymer matrix, drying kinetics, and water dynamics, all while looking at some existing models. They also concluded by pointing out the need for better uses of instrumentation and control.

This issue of microplastic formation from PAs in the ocean lead to an increasing interest in understanding the formation of these secondary microplastics. Grasping the mechanism will also allow us to control the reverse polymerization possibility of this type of plastic for circular and recyclable PAs. The hydrolytic degradation of PAs in aqueous solution at high temperature has been researched extensively for the past decades [22–46]. Nevertheless, parts of the research on the matter assume that with an aging temperature above 50 °C, hydrolysis is not simply dominant over oxidation, but renders oxidation entirely negligible [47]. The rest of the research simply disregards it. For the study of pure hydrolysis, the PA must be immersed in a carefully deoxygenated aging chamber. Several research articles do target pure hydrolysis as the sole mechanism of degradation; nevertheless, the more data gathered, the more confusing the overview. This lack of data compilation leaves room for a literature review focusing on this matter.

To achieve a full state-of-the-art comprehension of the pure hydrolysis of PAs, only papers explicitly stating that oxygen is removed from the aging chamber are reported here [1,8,48–69]. Several of the reported articles also aged their PAs under pure thermal oxidation and hydrothermal oxidation. These data are providing even further context to the degradation mechanism of PAs aged in deoxygenated water. They help placing hydrolysis contextually. This review focuses on the changes in molecular weight, crystallinity, chemical structure, and mechanical strength as individual chapters resulting from the pure hydrolysis of PA to draw out a state-of-the-art overview. Additionally, the impact of fibers, additives, pH, longer aliphatic chains in the PAs, correlation between molecular weight and crystallinity ratio, and the factor indicating embrittlement are discussed as well. This work is intended to help scientists grasp the full picture of the current research, which may assist them in either finding a research gap or comparing their own data to the current published literature without having to dive into dozens or even hundreds of papers.

2. Molecular Weight

2.1. Polyamide 6

PA6 has many intrinsic valuable properties such as high mechanical strength, high chemical resistance, low friction coefficient, and transparency. The polymer is not unaffected by water degradation due to the polarity of its amide bonds, which ultimately impacts its molecular weight overtime [70]. The molecular weight measurements presented here are all originating from gel permeation chromatography (GPC) measurements. Arhant et al. [52] immersed a 5 mm thick commercial PA6 containing a 60 wt% carbon fiber (C) reinforcement in water for up to 90 days with temperatures ranging from 100 °C to 140 °C. The changes in the number average molecular weight (M_n) of the polymer over time are shown in Figure 1. Starting at 26.2 kg/mol, M_n quickly drops within the first days and slowly reaches an equilibrium over time. For an aging temperature of 120 °C, M_n decreased from 26.2 kg/mol to 15.5 kg/mol within the first 10 days of aging, until reaching an equilibrium at around 11.0 kg/mol after 28 days. Increasing the aging temperature has two separate effects on M_n. Higher temperatures accelerate the decrease in M_n during the early-stage hydrolysis as well as the lowering of M_n at equilibrium. At 140 °C, the equilibrium was reached after only 9 days with a M_n of 8 kg/mol.

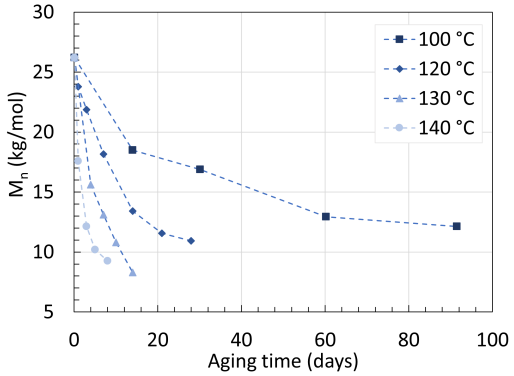

Figure 1. Changes in M_n of PA6/C over time at 100, 120, 130, and 140 °C when immersed in water. Data from [52].

On top of the M_n, the polydispersity index (PDI) or the distribution of molecular mass in a polymer was recorded as well. The PDI remained constant at 2.3 all throughout the process, indicating that pure hydrolysis is a random process occurring at all locations of the chains.

To investigate the coupling effect of hydrolysis and oxidation, Deshoulles et al. [48] aged their 0.25 mm thick neat PA6 material in dry hot air, deoxygenated water, and oxygenated water at 80 °C for long periods of time. Their GPC data are presented in Figure 2. The starting M_n was 52.3 kg/mol for all three degradation mechanisms. In deoxygenated water, M_n reached 32.5 kg/mol after 700 days of aging. In dry hot air, M_n reached 13.8 kg/mol after 630 days, making thermal oxidation a faster degradation process than pure hydrolysis at 80 °C. And finally, when immersed in oxygenated hot water, M_n fell drastically down to 13.5 kg/mol after merely 28 days, 80 times faster than pure hydrolysis. This underlines the importance of carefully removing oxygen from the aging chamber both in the solution and above it. The PDIs recorded for all three mechanisms are all dissimilar to one another. Similar to the previous data from Arhant et al. [52] as well as an earlier work from Deshoulles et al. [56], the PDI for pure hydrolysis at 80 °C remained at 2.3 constantly. For thermal oxidation, the PDI rose from 2.3 to 2.9 after the 630 days of aging. The authors issued this phenomenon to the cross-linking taking place at the last stage of oxidation. The PDI rose to even higher values when both mechanisms were combined. A PDI of nearly 4.5 after the 28 days of aging was reported, indicating that the chain scission process occurs in a less random manner compared to pure hydrolysis.

To decouple both mechanisms further, a sample of neat PA6 was aged in dry hot air until molecular weight equilibrium, then placed in deoxygenated hot water. We note that the equilibrium reached when aged under oxidation and hydrolysis is different, as oxidation includes radical chemistry which leads not only to the formation of amines and carboxylic acids, but also cross-linking, bridging, and more. The results are shown in Figure 3. Both mechanisms were taking place at 100 °C to accelerate the procedure. The M_n decreased further even after the pre-oxidative treatment. This phenomenon is linked to the formation of imides during oxidation before chain scission, enhancing the likelihood of hydrolysis occurring from these chemical groups. This has been proven through Fourier-transform infrared (FTIR) spectroscopy. The infrared spectra are discussed further in Section 4.

When comparing the decrease in M_n of PA6/C and neat PA6, one can notice the significantly slower drop in M_n of the neat PA6 over time. At 80 °C, the neat PA6 obtained a M_n 32.4 kg/mol after 700 days of aging, compared to the PA6/C that reached a M_n of 12.1 kg/mol after only 90 days of aging at 100 °C; both reached equilibrium. The fibers were described by Arhant et al. [52] as being indifferent to both the effect of water and temperatures as high as 120 °C. Hence, the contrast may originate solely from the small difference in aging temperature, pointing out that an exponentially higher degradation rate occurs with aging temperatures higher than 80 °C for PA6. This indication is further

supported by looking at an earlier work from Deshoulles et al. [56], where, again, neat PA6 with a thickness of 0.25 mm was aged in deoxygenated water, but at 120 °C until equilibrium. Both trends are shown in Figure 4. The M_n of both PA6s decreases to a similar value. Notably, a higher starting M_n also seems to result in a faster degradation rate. In the case of glass fibers, the presence of reinforcement has been associated to a lower water absorption property due to the simple fact that less PA is present in the network when reinforced [26]. If the two PA6 were to start at similar M_n, it is likely that the reinforced PA would degrade slower.

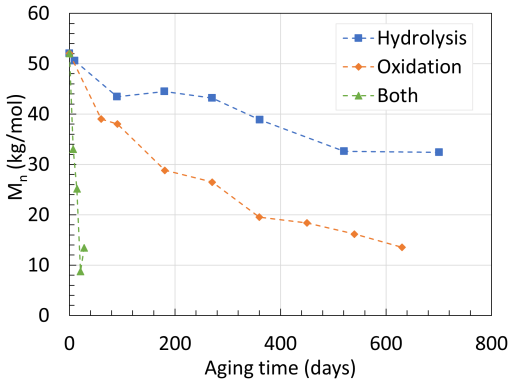

Figure 2. Changes in M_n of neat PA6 over time and degradation mechanisms at 80 °C. Data from [48].

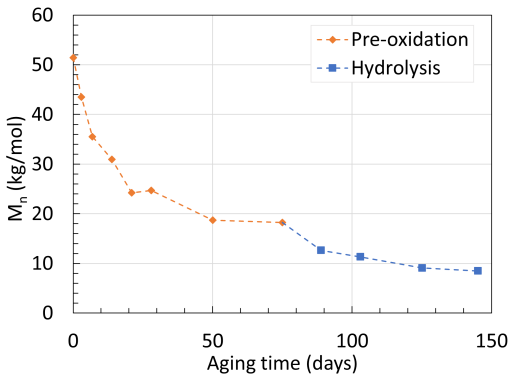

Figure 3. Changes in M_n of neat PA6 over time with a pre-oxidative stage at 100 °C. Data from [48].

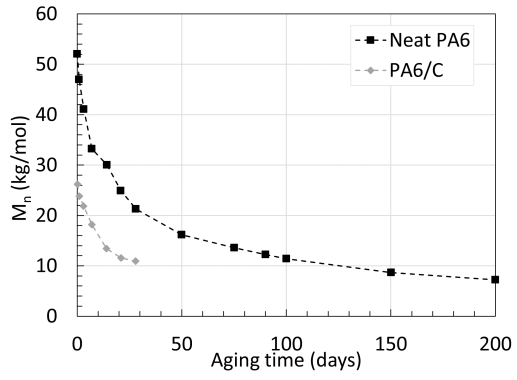

Figure 4. Changes in M_n for neat PA6, and PA6/C at 120 °C for up to 200 and 28 days, respectively. Data from [52,56].

Another earlier work from Deshoulles et al. [55] aimed at determining a parameter able to track the embrittlement or, i.e., the ductile to brittle transition of PA6. Neat PA6 without additives was aged in deoxygenated water and dry hot air separated once again for up to almost 2 years with temperatures ranging from 80 °C to 140 °C. The samples

had a thickness of 250 µm and 75 µm, respectively. The PDI recorded from aging through both pure hydrolysis and pure thermal oxidation remained equal to 2.5 ± 0.5. This high deviation created a large uncertainty, preventing a direct comparison to other PDI values from other sources. The changes in M_n are shown in Figure 5 for both pure hydrolysis and Figure 6 for pure thermal oxidation.

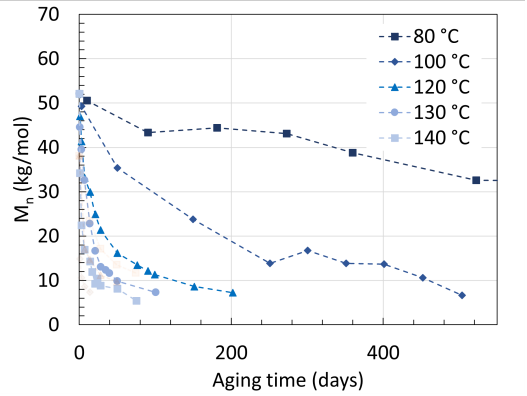

Figure 5. Changes in M_n for neat PA6 without additives in deoxygenated water with varying temperatures. The dotted lines are here for illustrations and does not represent a mathematical fitting. Each reaction temperature has a shape and symbol respectively. The see-through plot in the background corresponds to the data for oxidation. Data from [55].

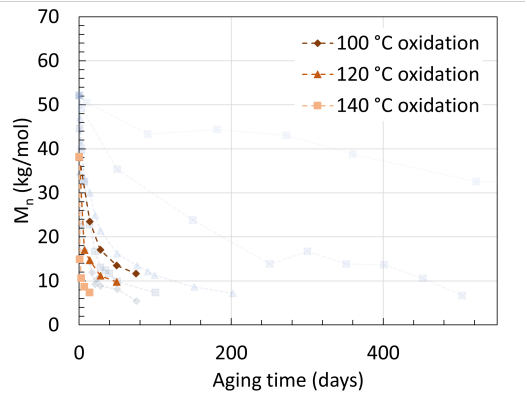

Figure 6. Changes in M_n for neat PA6 without additives in dry hot air with varying temperatures. The dotted lines are here for illustrations and does not represent a mathematical fitting. Each reaction temperature has a shape and symbol respectively. The see-through plot in the background corresponds to the data for hydrolysis. Data from [55].

Degrading PA6 in dry air led to a faster drop in M_n than degrading it in deoxygenated water at high temperatures. For pure hydrolysis, M_n reached 32.6 kg/mol after 520 days of aging at 80 °C, and this value decreased exponentially to 6.7 kg/mol when rising the temperature from 80 °C to 100 °C for about the same aging time. This is in correlation with the previous statement that a significant effect is to be expected at the 80 °C to 100 °C temperature range. Increasing the temperature further led to a faster drop rate and a slight decrease in M_n at equilibrium.

2.2. Polyamide 11

In addition to PA6, knowing the degradation behavior of PA11 in deoxygenated water has also been of great interest. This comes from one of its main applications as internal pressure sheath in offshore underwater flexible pipes where the concentration of oxygen is scarce [51]. PA11 harbors a high chemical resistance, with a working temperature ranging from −40 to 130 °C. [71]. PA11 also undergoes hydrolysis like PA6 or PA66. The main difference lies behind PA11's water affinity worsened by its longer carbon chain. Meyer et al. [68]

aged an unplasticized, laboratory-made 3 mm thick neat PA11 in deoxygenated water at temperatures ranging from 90 °C to 135 °C with varying starting average molecular weight (M_w). The M_w is another way of describing the molecular weight of polymers and is always greater than M_n. Factoring the M_n with the PDI provides M_w. The variations of M_w over time at 90 °C and 135 °C are displayed in Figure 7.

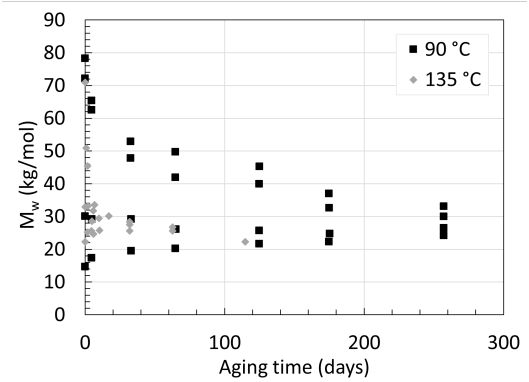

Figure 7. Changes in M_w for neat PA11 at 90 °C and 135 °C for up to 260 days. Data from [68].

Regardless of the starting M_w, all M_w values tend towards an equilibrium. The accelerating effect is more than obvious when looking at the M_w after around 65 days of aging for both 90 °C and 135 °C with 72 kg/mol as a similar starting M_w. At 90 °C, M_w reached about 50 kg/mol, while at 135 °C, this value reached 25 kg/mol. One can argue visually that the M_w at equilibrium for 135 °C tends towards 25 kg/mol, and for 90 °C, this equilibrium appears to be at around 28 kg/mol. This would be in line with the previous statement regarding the effect of temperature on PA6 upon its M_n. Another important information is the fact that all PA11s with a starting M_w below the equilibrium have their M_w rising towards it. This increase in M_w is another sign of the reaction equilibrium between hydrolysis and condensation. M_w below such equilibrium implies a higher concentration of primary amine and carboxylic acid end-groups in contrast to the concentration of amide groups in the polymer. Following the basic concept of the Le Châtelier's principle, this shift induces an enhanced condensation rate of the end groups. Meyer et al. [68] also looked at the effect of pH by aging the same PA11 in acidic aqueous solution with a pH of 3 and 5 using hydrochloric acid. The lower the pH, the faster the hydrolysis rate, and the lower the M_w. At pH 5, the equilibrium shifted from 25 kg/mol to around 22 kg/mol at 120 °C. The effect of lower pH is said to protonate the amine end groups to a cation. This ties up the lone pair of electrons initially present on the nitrogen group, preventing the nucleophilic attack of the amine towards the carboxylic acid. This explains the lower condensation rate and the lower M_w at equilibrium at lower pH.

Similar results were obtained from the work of Hocker et al. [59]. Samples of 0.3 mm thick PA11 plasticized with an unspecified amount of N-butylbenzenesulfonamide (BBSA) were aged with different amounts of graphene oxide (GO) as reinforcement at 100 °C and 120 °C for up to 4 months. Without any fibers, the M_w reached around 24 kg/mol at equilibrium for both temperatures, and the higher aging temperature caused the expected accelerating effect reported several times previously. The increased aging temperature did not lower the M_w significantly, probably due to the lower impact of hydrolysis on PA11 compared to PA6 and the small temperature difference of merely 10 °C. At 100 °C, the hydrolysis rate and condensation rate reached 2.8×10^{-2} and 5.0×10^{-5} day^{-1}. These rates increased to 12×10^{-2} and 23×10^{-5} day^{-1} for 120 °C, according to the authors' data. Additionally, 1 mg/g of GO in PA11 rose M_w at equilibrium by 40% from the neat PA11 for both temperatures and reduced the hydrolysis rate by 1×10^{-2} day^{-1} at 100 °C and 7.5×10^{-2} day^{-1} at 120 °C. However, 5 mg/g resulted in the loss of that property from a poor nano-particle dispersion due to agglomeration of the GOs.

Jacques et al. [69] degraded their 3 mm thick 12 wt% BBSA plasticized samples with additional light and heat stabilizers in deoxygenated water for 450 days with temperature ranging from 90 to 140 °C. The viscosity was also tracked using rheology. Only the full graph for the degradation at 140 °C was provided from GPC. The M_n at equilibrium was provided for the other aging temperature. For PA11, the PDI recorded during pure hydrolysis was always around 1.9, unlike the 2.3 from PA6. The hydrolysis rate rose from 0.42×10^{-4} kg · mol^{-1} × day^{-1} at 90 °C to 24.1×10^{-4} kg · mol^{-1}· day^{-1} at 140 °C. It was found that the rate of condensation was 1000 faster than hydrolysis when M_n or M_w were under equilibrium, and this increased exponentially as temperature decreased below 90 °C. We note that this was calculated from the temperature domain of this study. The data from PA11 aged at 140 °C were obtained from Jacques et al. [69], and the data from Hocker et al. [59] at 100 °C, and 120 °C are displayed in Figure 8 below. Figure 9 displays M_n at equilibrium recorded from Jacques et al. [69] but converted to M_w for easier comparison using their recorded average PDI of 1.9 at 80 °C after aging.

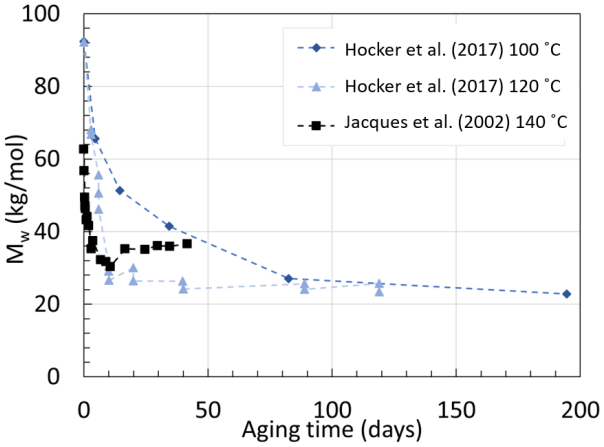

Figure 8. Changes in M_w for plasticized PA11 aged at 100 °C, 120 °C, and 140 °C. Data from [59,69].

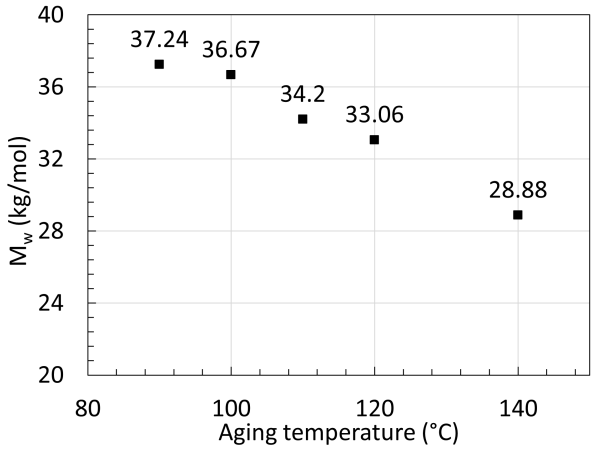

Figure 9. Series of reached M_w at equilibrium from aged PA11 at varying temperatures. Data from [69].

The data from Jacques et al. [69] showed that at 140 °C, the M_w decreases fast as expected within the first days, but seems to reach a much higher M_w at equilibrium than the two neat PA11 from Hocker et al. [59] at 100 °C and 120 °C. This was not discussed by the authors. Both PA11 contain plasticizers and additives but likely not in the same quantity. Jacques et al. [69] mentioned that the polymer contained an unspecified amount of heat and light stabilizer as opposed to the ones from Hocker et al. [59]. The decrease and subsequent increase in M_w may arise from the extraction of such additives.

On top of that, the M_w at equilibrium for 140 °C calculated from their tables is lower than the measurements from their graph. The calculated 28.88 kg/mol was found with the

assumption that the PDI would remain the same, regardless of the aging temperature. If one takes the direct M_n at equilibrium and the M_w at equilibrium from the graph, a PDI of about 2.3 is calculated. When looking at the data from Meyer et al. [68], this PDI seems to sit at a lower value, closer to 1.6.

Another paper experimenting on the degradation of PA11 in water worth mentioning looked at the changes in M_n and M_w over time and degradation mechanisms. There, Maïza et al. [57] aged their 1.5 mm to 2.0 mm thick PA11 in deoxygenated hot dry air and deoxygenated hot water. The data for both conditions did not differ much and, in them, hydrolysis resulted in a faster reduction in M_w compared to thermal degradation. The authors detected the presence of free radicals formed during the extrusion via FTIR, showcasing the importance of carefully preventing the formation of free radicals from any parts of the experiments, not solely the aging process.

The effect of pH has been briefly mentioned before, but not extensively. When one thinks of reducing the pH of an aging chamber, hydrochloric acid [68,72] or sulfuric acid [73] are often used. An earlier work from Hocker et al. [61] investigated the possibility of using organic acids instead. The authors found that not only do organic acids degrade PAs faster than inorganic acids, but the weaker the organic acid, the faster the degradation. This was attempted with acetic, propanoic, and butanoic acid at a concentration of 1.05×10^{-2} M for all three on their 250 mm to 1 cm laboratory-made thick PA11 sample. For PA11 aged in water, M_w at equilibrium reached 24.4 kg/mol and 26.9 kg/mol for 100 °C and 120 °C respectively. The higher M_w is likely an exception occurring from the small temperature difference. The rate of hydrolysis, on the contrary, increased from 0.43×10^{-1} to 1.64×10^{-1} from the temperature increase, proving again that the main effect of temperature is acceleration. Another experiment from Hocker et al. [58] was designed to determine the ductile to brittle transition. In this attempt, they also aged two PA11 samples with a thickness of 2 ± 0.5 mm and 0.3 ± 0.02 mm in water, acetic acid, and butanoic acid at 120 °C. As the data originate from the same research group and consist of the same experimental setup, the results are combined and depicted in Figure 10. At 120 °C, the M_w of neat PA11 at equilibrium reached 26.9, 20.0, 17.0, and 14.5 kg/mol when aged in water, acetic, propanoic, and butanoic acid solutions. Acids have two effects on degradation, a hydrolysis acceleration effect as well as an amine scavenging effect. The solubility of the acid in regard to the PA is the governing factor, not its pH.

This is well represented in Figure 11, where the variations of M_w over time of plasticized PA11 aged in different acidic conditions are shown.

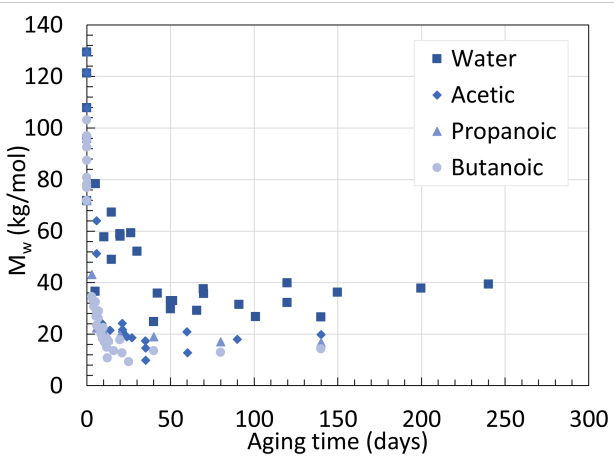

Figure 10. Variations of M_w for PA11 in different acidic conditions at 120 °C. Data combined from both works of Hocker et al. [58,61].

The M_w of PA11 dropped faster and reached lower values when aged in acetic acid than hydrochloric acid, despite their similar pH. Plasticized PA11 resists well against the

effect of degradation due to BBSA disrupting the hydrogen bonding matrix in PA11. The correlation between M_w or M_n and mechanical properties is investigated in Section 5.

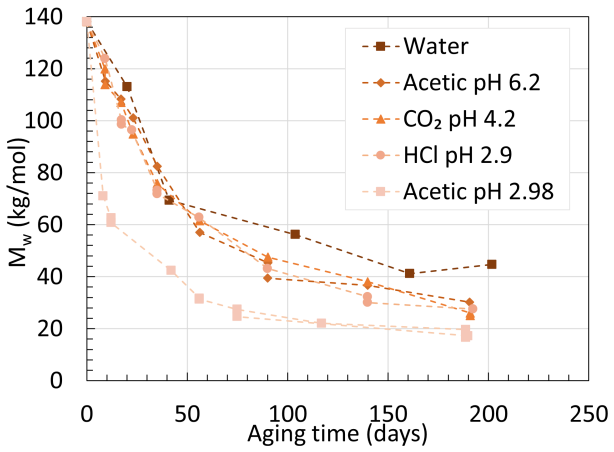

Figure 11. Variations of M_w for stabilized PA11 in different acidic conditions at 100 °C. Data from the second work of Hocker et al. [58].

3. Crystallinity

3.1. Polyamide 6

The data presented here are only obtained from differential scanning calorimetry (DSC) measurements. The second heating scans and crystallinity ratios (X_c) over different aging times of 5 mm thick PA6/C from Arhant et al. [52] are shown in Figures 12 and 13, respectively. The X_c from the original paper was calculated from a melting enthalpy of a 100% crystalline PA6 of 118 J/g, though this value must be similar for all papers to compare results. Hence, the X_c is calculated from 240 J/g instead, which is the standard used by the rest of the sources in this section as well as another paper describing the crystallization behavior of carbon fiber-reinforced PA6. [74]

Looking at the thermograms, the shape of the scans is unaffected by the increasing aging time at 120 °C. The X_c, on the other hand, is affected drastically as the polymer ages and the temperature rises. At 140 °C, the X_c rises from 18.7% to 26.7% after only 9 days. This is significantly faster than aging the polymer at 100 °C, rising the X_c from 18.7% to 23.5% only after 90 days.

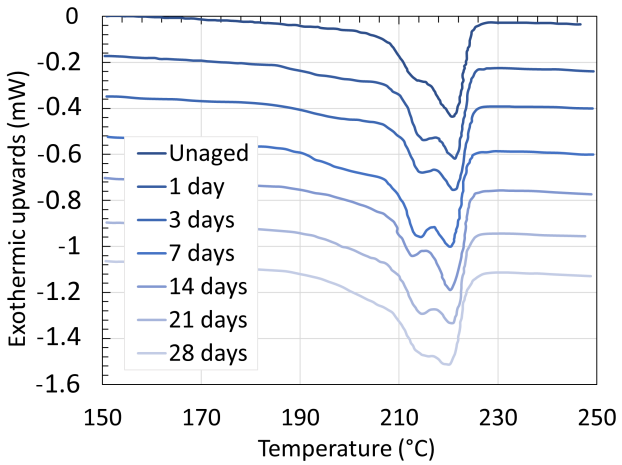

Figure 12. Second heating scans of PA6/C as a function of time at 120 °C. Data from [52].

The rise in X_c is the result of chemi-crystallization, a physical process in which the shorter polymer chains, resulting from chain scission, obtain higher mobility within the

matrix. This allows them reorganization of themselves from a disordered amorphous phase into new crystallites. The authors also state that the carbon fibers are not impacting chemi-crystallization as they are known to only impact the crystallinity on the polymer melt. The increase in X_c looks like the decrease in molecular weight, converging towards a maximum value. The activation energy calculated from the crystallinity ratio is found to be 113 kJ/mol.

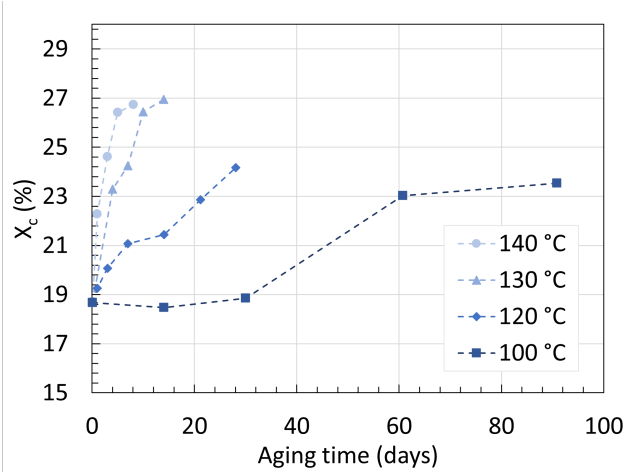

Figure 13. Variations in X_c of PA6/C as a function of time and temperature. Data from [52].

The variations of X_c of 0.25 mm thick neat PA6 at 80 °C from Deshoulles et al. [48] when aged under thermal oxidation, pure hydrolysis, and hydrothermal oxidation are shown in Figure 14. The X_c value rises from 20 to 29% after 620 days of thermal oxidation, 32% after 700 days of pure hydrolysis, and 30% after only 21 days of hydrothermal oxidation. The increase in X_c is exponential within the first day, and to some extent the first few minutes of aging except for thermal oxidation where the increase is slightly more linear. This is attributed to the formation of a monoclinic crystalline α-phase in hot water, a process separate from chemi-crystallization. Crystallinity in semi-crystalline polymers like PAs is originating from the hydrogen bonds of their amide groups. As the number of hydrogen bonds increases, so does X_c. Water rearranges these bonds by also creating additional hydrogen bonds within an amorphous matrix [26,75]. This results in a faster and stronger increase in X_c despite a slower rate of degradation, as shown when comparing the data to thermal oxidation.

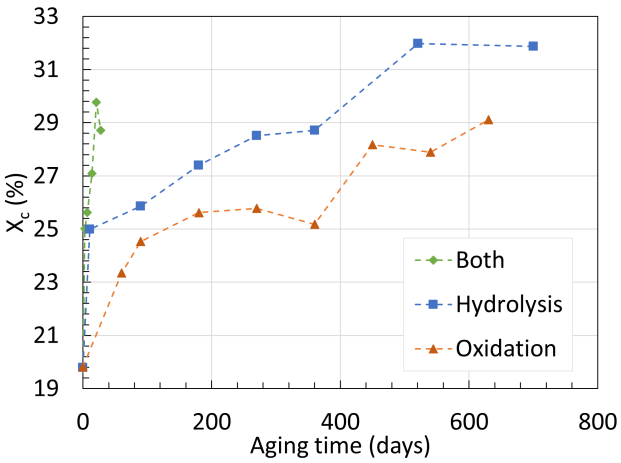

Figure 14. Changes in X_c of neat PA6 over time and the three different degradation mechanisms investigated at 80 °C with a starting X_c of 20%. Data from [48].

By using M_n and X_c, the concentration of chain scission in the amorphous phase can be calculated. This is performed to quantify the degradation at the macromolecular scale using

the following formula: $S_a = \frac{1}{1 - X_c} \cdot (\frac{1}{M_n} - \frac{1}{M_{n0}})$, where S_a is the concentration of chain scission in the amorphous phase. These concentrations are displayed in Figure 15. The data are extracted from aging at 100 °C. In a similar fashion as X_c, S_a increases exponentially within the first day of aging and slows towards a maximum value later. Here, pure hydrolysis is shown to have a lower S_a than thermal oxidation, which is in accordance with the general agreement that thermal oxidation degrades PAs faster than pure hydrolysis.

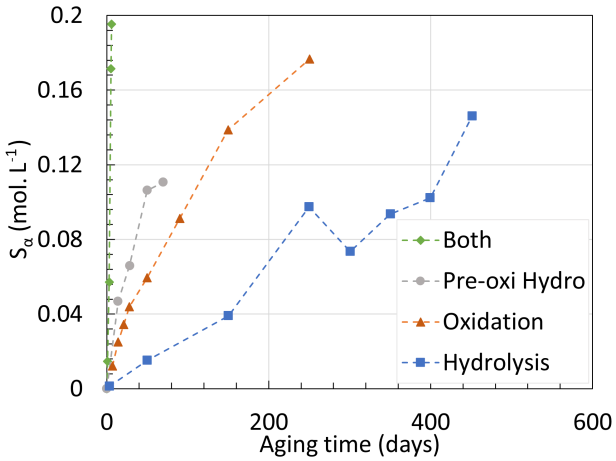

Figure 15. Concentration of chain scission in the amorphous phase of neat PA6 over time and degradation mechanisms at 100 °C. Data from [48].

Deshoulles et al. [48] also calculated S_a for pure hydrolysis after 75 days of pre-oxidation. For that mechanism, S_a is higher than pure hydrolysis and thermal oxidation but still lower than hydrothermal oxidation. The reason remains the same; oxidation products like imides enhance hydrolysis by presenting more lone pairs from the carbonyl group to be attacked by water molecules.

The fast increase in X_c within the first day of aging due to hot water was also shown for PA6 from an earlier work published by Deshoulles et al. [56]. The second heating scans are depicted in Figure 16. For comparison, the variations in X_c of PA6/C from Arhant et al. [52] and neat 0.25 mm thick PA6 from two publications of Deshoulles et al. [55,56] aged at 120 °C are shown in Figure 17.

The thermograms clearly display the increase in melting enthalpy (ΔH_m) when looking at the integral of the signal at around 220 °C. It also seems like the already appearing second shoulder at 210 °C is increasing in size. This is slightly similar to the second heating scans of PA6/C in Figure 12. In an interesting way, the second heating scans of PA6 denote two melting peaks for the unaged sample, like PA66. The first melting peak is said to be attributed to the thin lamellae formed from the cooling phase, whereas the second melting peak is formed from the melting of the thickened crystals during the heating phase [76].

The drastic increase in X_c during the first minute of immersion has been issued to the formation of a monoclinic phase induced by hot water. To be more precise, Deshoulles et al. [55] described it as the transition from a β-amorphous to a monoclinic α-phase, based on their wide-angle X-ray scattering analysis. This is only possible in water as when applied to thermal oxidation under the same parameters, the same results are not shown [55,56,75,77]. This phase transition is likely directly linked to plasticization. After the rapid increase in X_c from 20% to 35% for both neat PA6, X_c keeps on slowly increasing to an average of 50% due to chemi-crystallization. Interestingly, the data are identical for both neat PA6 sources until the very last measurement, which is not further discussed in the original literature.

The X_c of PA6/C started at lower values than neat PA6 and further increased in a linear fashion, as opposed to the drastic exponential rise from the neat PA6. One major difference is the large thickness of the PA6/C sample; it was 20 times thicker. This likely

means that the matrix of PA6/C is not water saturated, creating a diffusion gradient which ultimately slows down the degradation process. Additionally, the effect of reinforcement in PAs upon hydrolysis has been shown to reduce water absorption [26]. The water content of PA6/C increased from 0% to 5% within the first day of aging, while the water content of neat unreinforced PA6 increased from 0% to nearly 12.5% after similar aging time. This confirms the previous statement.

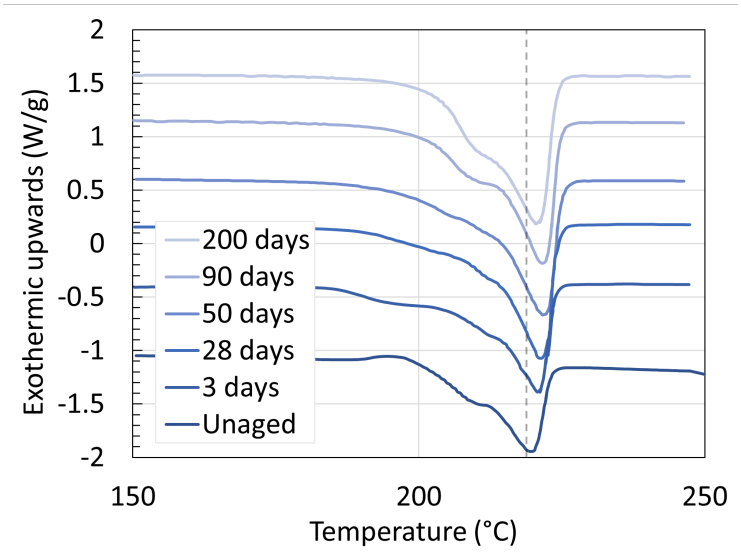

Figure 16. Second heating scans of neat PA6 with varying aging time at 120 °C. Data from [56].

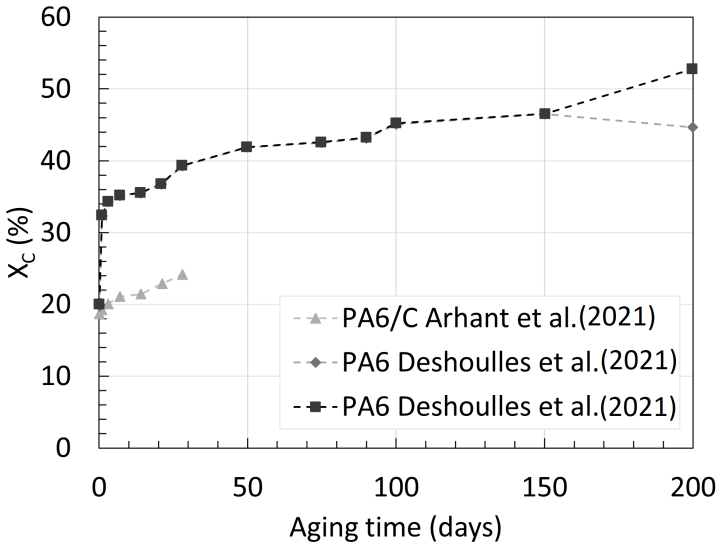

Figure 17. Variations of X_c for PA6/C and neat PA6 over time at 120 °C. Data from [52,55,56].

Rising the aging temperature causes the X_c to rise faster and to higher values, as seen with the data from Arhant et al. [52]. Similar setup for neat PA6 from Deshoulles et al. [55] was performed in both deoxygenated water and dry air. The corresponding data are presented in Figure 18 and Figure 19, respectively. Despite a slower degradation of PA6 under pure hydrolysis, the measured X_c reached higher and faster values than that of degradation under thermal oxidation. At 80 °C, X_c appears to converge towards about 33% after 600 days of aging. However, at 140 °C, X_c rises to values higher than 60% after about 100 days of aging, and this value does not appear to reach an equilibrium. This is extremely interesting as this behavior is relatively dissimilar to the changes in molecular weight, where all trends converge towards a similar value regardless of the aging temperature.

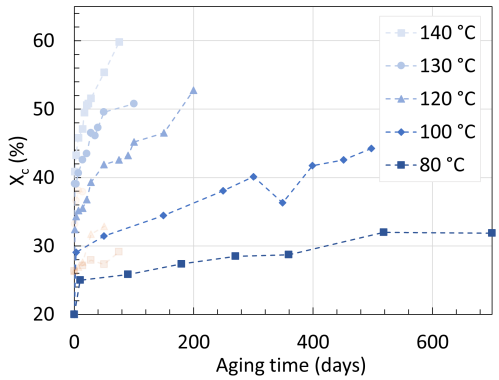

Figure 18. Variations of X_c for neat PA6 over time at different temperature under pure hydrolysis condition. The dotted lines are here for illustrations and does not represent a mathematical fitting. Each reaction temperature has a shape and symbol respectively. The see-through plot in the background corresponds to the data for oxidation. Data from [55].

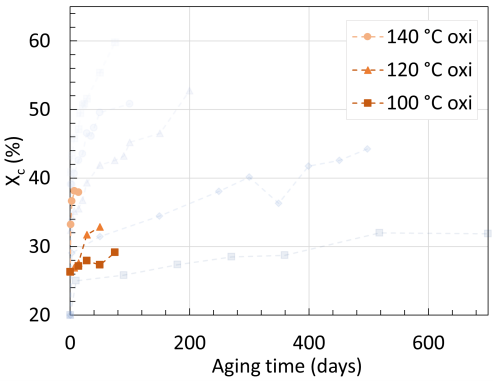

Figure 19. Variations of X_c for neat PA6 over time at different temperature under thermal oxidation condition. The dotted lines are here for illustrations and does not represent a mathematical fitting. Each reaction temperature has a shape and symbol respectively. The see-through plot in the background corresponds to the data for hydrolysis. Data from [55].

3.2. Polyamide 11

According to Da cruz et al. [50], reinforcing 0.1 mm thick PA11 with 1.0, 2.5, and 5.0 wt% graphene nanoplatelets has a negligible effect upon the polymer's crystallinity at the start. Regardless of the degree of reinforcement, X_c remained at 17%, that is, without any aging occurring yet. The authors also investigated the nature of the crystalline structures, and found that PA11 has five crystalline phases: triclinic α, monoclinic β, with three pseudo-hexagonal, a γ, a δ, and a δ' form, all measured through X-ray diffraction (XRD) analysis.

The influence of graphene oxide (GO) on the changes in crystallinity of 0.3 mm plasticized PA11 immersed in deoxygenated water was also investigated by Hocker et al. [59]. X_c for neat PA11 and reinforced PA11 with 1 and 5 mg/g of GO had a starting value of $25 \pm 1\%$ at first. Similar to the results obtained by da Cruz et al. [50], the presence of graphene reinforcement did not influence the starting X_c. After 90 days of aging at 120 °C, X_c increased from 25.4% to 32.3% for neat PA11, 31.1% for 1 mg/g GO reinforced PA11, and 27.0% for 5 mg/g reinforcement. This shows that the GO does hinder hydrolysis. It prevents it by competing with the hydrogen bonds of amides from PA11 and water molecules. The presence of reinforcement also impacts the water uptake ability of the PA.

Domingos et al. [62], Romão et al. [1], and Da costa et al. [51] presented the second heating scans of their stabilized aged PA11 from their DSC measurements in their article. Each PA11 had a respective thickness of 5.5 mm, 5.5 mm, and 7 mm. For the sake of comparison, these are shown side by side, respectively, in Figures 20–22.

The second heating scans of unaged PA11 for all three figures do not show the same two melting temperatures peak shown for unaged PA6 like in Figures 12 and 16 or even PA66. This may be indicative of the fact that PA11 does not rearrange the lamellae crystals as well as PA6 and PA66 do, if at all [76].

When observing the thermogram of PA11 aged at 110 °C for 50 days shown in Figure 20, a second melting temperature peak appears. This shoulder is the melting temperature of the newly formed oligomers from hydrolysis. This new melting peak is somewhat visible on PA11 aged in oilfield water at 120 °C with a pH of 5.5 after 50 days in Figure 21, and visible too for PA11 aged in salted water at 120 °C with a pH of 5.5 despite 109 days of aging in Figure 22.

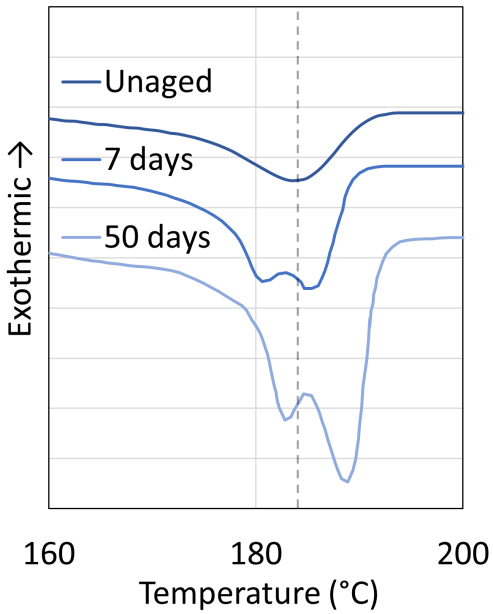

Figure 20. Second heating scans of PA11 aged in water at 110 °C at pH 7.0. Data from [62].

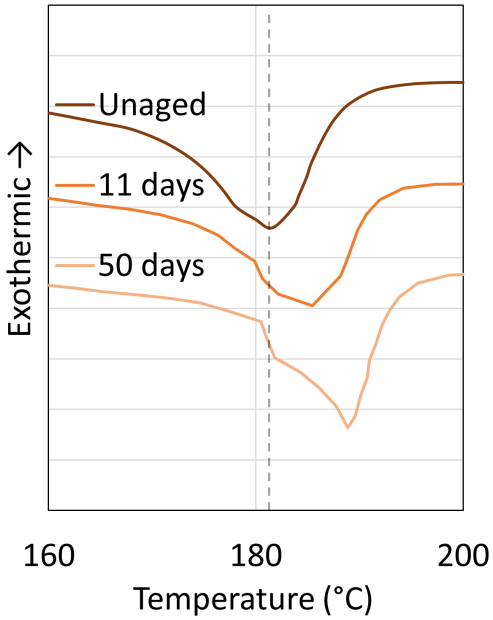

Figure 21. Second heating scans of PA11 aged in oilfield water at 120 °C at pH 5.5. Data from [1].

The two melting temperatures shift to higher values as aging progresses, interpreted by the authors as the formation of different sized crystals dispersed and homogenized in

PA11. We can notice this shift in melting temperatures for the other two thermograms. It also seems that the shift converges towards a similar value of 188 °C for all three scans. One source does indicate the plasticizer loss to be a potential variable [51].

We note that Da costa et al. [51] aged their PA11 in two solutions, one being a salt mixture containing compounds found in offshore oil production, and one similar but with a concentration four times higher of acetate and propionate ions. They display the exact same second heating scans, but different first heating scan. The first heating scan presented a shoulder increasing drastically in height at 175 °C after 71 days. This was assimilated to a crystal phase transition induced, also referred to as the Brill transition, which converts a triclinic α crystal phase into a metastable pseudo-hexagonal smectic δ' phase. The thermally induced pseudo-hexagonal phase disappears in the second heating scans, and the newly formed shoulder is attributed to the presence of smaller crystals formed by hydrolysis and plasticizer loss. The main shoulder in the first heating scan is also seen in the second one as the main peak, demonstrating a more permanent change. This corresponds to the α crystalline phase, and is the signal used to monitor the changes in crystallinity.

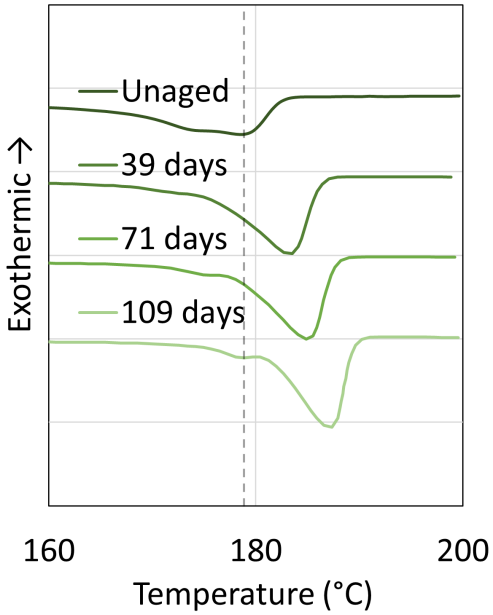

Figure 22. Second heating scans of PA11 aged in salted water at 120 °C at pH 5.5. Data from [51].

A publication from Maïza et al. [57], in which they failed to prevent the formation of peroxides through oxidation on their PA11, also confirmed the interpretation proposed by Da costa et al. [51].

Using the authors' ΔH_m data, X_c can be extracted for the aging experiment of PA11, as the authors do not display it themselves. However, ΔH_m for the standard 100% crystalline PA11 remains disputed. Da Costa et al. [51], Maïza et al. [57], da Cruz et al. [50], and Olufsen et al. [54] used a ΔH_m of around 226 J/g [78], which is in agreement with other sources [79–81], while Hocker et al. [58,59] used 189 J/g [82] in their articles. Some other literature work [83–87], irrelevant to the topic of pure hydrolysis of PAs, used a ΔH_m of 206 J/g as reference. Based solely on the amount of sources, the most accurate value is likely between 206 J/g and 226 J/g. Using a different standard for assessing X_c does not hinder the end result of one set of data. However, we have to remain careful and aware of that when cross-analyzing different X_c data.

When 226 J/g as the standard ΔH_m for a 100% crystalline PA11 was used, X_c rose from 10% to 20% for both solutions after 109 days of aging at 120 °C. We note that the authors accounted for the mass of plasticizer in their X_c calculations. Using the same reference, Domingos et al. [62] had their X_c rise from 14.6% to 19.5%, close to the data by Da costa et al. [51] yet showing dissimilar second heating scans.

The cooling scans of aged PAs also draw interesting information. The scans from Domingos et al. [62] and Romão et al. [1] are shown in Figures 23 and 24, respectively. The displayed peaks represent the crystallization temperature (T_c) of PA11. T_c values are different for both unaged PA11; however, after 50 days of aging, they both shift to a similar higher value, all while presenting a narrower signal. This is said to be yet again originating from the formation of lower molar mass oligomers from the amorphous phase migrating to the crystalline phase [1,62,88,89].

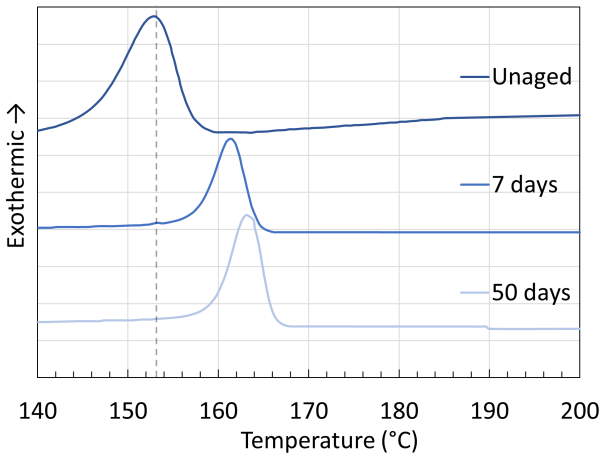

Figure 23. Cooling scans of PA11 aged in water at 110 °C at pH 7.0. Data from [62].

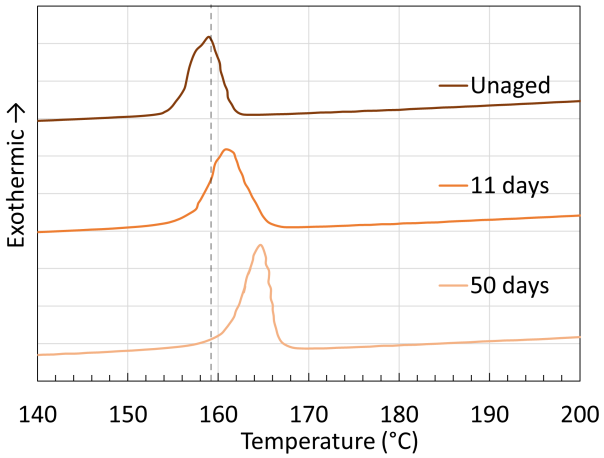

Figure 24. Cooling scans of PA11 aged in oilfield water at 120 °C at pH 5.5. Data from [1].

Hocker et al. [58] aged their two 2 ± 0.5 mm and 0.3 ± 0.02 mm thick PA11 samples with 12.5 wt% BBSA at 120 °C in aqueous organic acid to determine the most suitable parameter to track the ductile to brittle transition, i.e., embrittlement. The changes in X_c are depicted in Figure 25. For contrast, Domingos et al., [62] also measured the ΔH_m of their aging PA11, hence the converted X_c values are shown in Figure 25.

We can immediately notice the slower increase in X_c for PA11 aged in water at 110 °C and 120 °C from Domingos et al. [62] compared with the one from Hocker et al. [58] aged in water at 120 °C. The only contrast is the sample thickness being larger for the two PA11. The larger thickness causes an absorption gradient in the PA11 matrix, causing water to take a lot longer to diffuse through the entire sample, thereby causing a slower degradation rate portrayed by a slower rise in X_c.

The slope of the increase in X_c in the first stage of aging is steeper as the organic acid weakens or resembles the chemical structure of the polyamide in question. X_c was calculated from the standard ΔH_m of 226 J/g. For water, X_c rose from 15.5% to about

35.8% after 240 days. This comparison cannot be made with the acid measurement as it was stopped long before. Acids have a catalysis and amine scavenging effect, proven by the molecular weight data. The catalysis effect can be seen here, though the amine scavenging effect cannot be determined as the plateau has not been reached for both acids. Nevertheless, the plateau for butanoic acid does seem to lay above the one of water. We note that like other DSC data, X_c does not converge in a similar way as M_n.

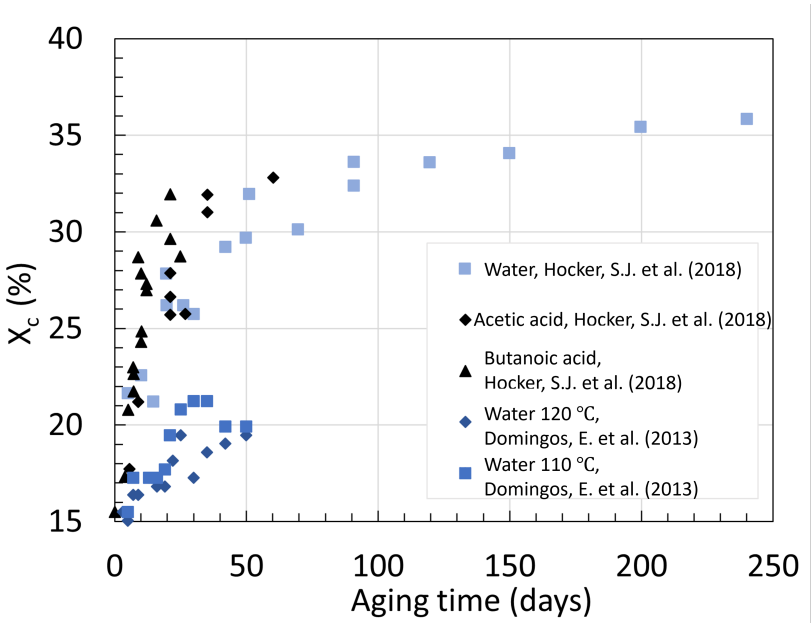

Figure 25. Variations of X_c for plasticized PA11 over time at 120 °C with different organic acids, along with another plasticized PA11 aged in water at 120 °C and 110 °C. Data for water, acetic, and butanoic acid from [58] and for water at 110 and 120 °C from [62].

At 120 °C, the plasticized PA11 from Hocker et al. [58] had its crystallinity rise from 15.5% to about 35.8% after 240 days. At the same temperature, PA6 from [55] rose from 20% to about 52% after 200 days of aging. While the BBSA present in PA11 reduced this percentage, we can notice how high of a value X_c can reach. The longer aliphatic chain in PA11 ultimately results in a slower and weaker raise in X_c when aging at the same temperature and time.

4. Chemical Analysis

4.1. Polyamide 6

As degradation occurs, the long polyamides chains are cut into shorter oligomers with amines and carboxylic acid end groups. Among the papers, Fourier transform infrared spectroscopy (FTIR) has been used several times to track the changes in chemical groups of the polymers. In a paper by Alam [67], ^{17}O nuclear magnetic resonance (NMR) was performed on PA66 to track quantitatively the amount of carboxylic acid groups formed as a function of degradation. This work, however, does not properly control the oxygen content of the aging salt solution, implying that the combination of hydrolysis and thermal oxidation was occurring. Despite that, Alam found that the carboxylic acid group rose in number as aging progressed.

FTIR can also be used for qualitative and quantitative analysis. By applying the same baseline for all specimen graphs and the correct internal reference, we can measure the integral of the band associated with an identified functional group and quantify it. As the Beer–Lambert law states, the radiation absorbance band of a functional group, or chromophore, is proportional to its concentration [90]. Deshoulles et al. [48] used FTIR on their PA6 samples, and the results are shown in Figure 26 for their samples aged in deoxygenated water.

At first glance, we can notice a lack of strong differences between spectra in Figure 26 despite 700 days of aging, displaying the difficulty of tracking the chemical changes occurring through the pure hydrolysis of nylon. For PA6 samples subjugated to pure hydrolysis, a decrease in the bands located at 3292, 1634, and 1538 cm^{-1} are seen. These correspond to secondary N–H stretch, C=O amide I and II, and are the result of the depletion of amide groups in the amorphous phase. Not only are some of the bands showing the absorption of a certain functional group, but the crystalline nature of these bands is also sometimes possible to determine. According to the authors, the band at 2926 cm^{-1} assigned to asymmetric C–H_2 amorphous decreases in intensity while the one at 2916 cm^{-1} assigned to asymmetric C–H_2 crystalline increases in intensity. This is also seen for the symmetric ones at 2869 and 2856 cm^{-1}. These, however, are relatively hard to see in the figure.

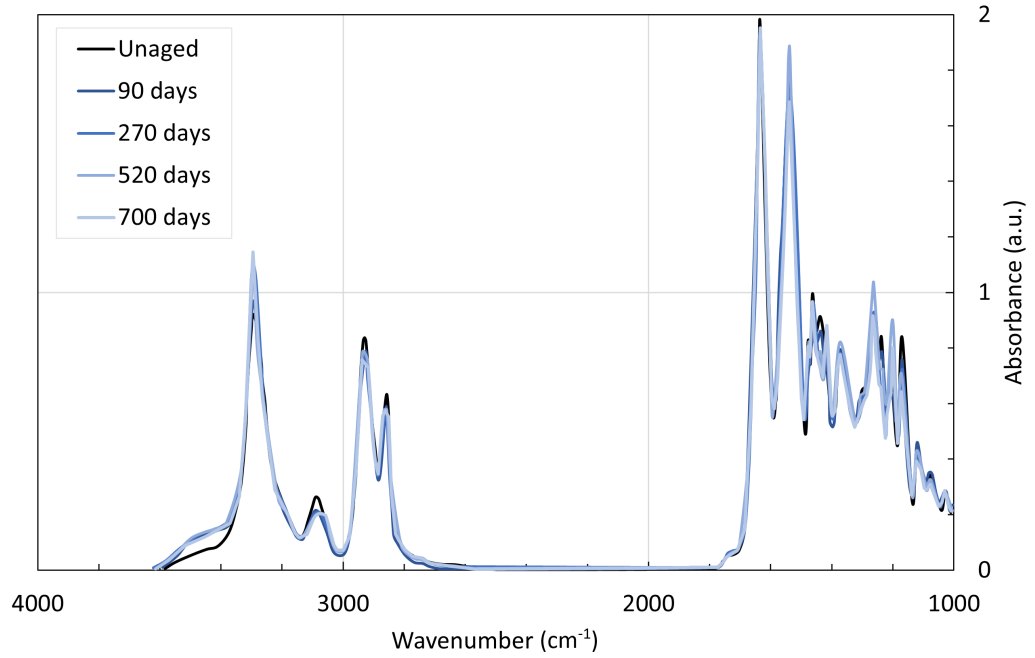

Figure 26. Infrared spectra of PA6 aged in deoxygenated hot water at 80 °C over time. Data from [48]. We note that, as the spectra were stacked on top of each other, the data extraction was trivial, and some minor negligible variations may be present.

The rise of the signal assigned to hydrogen bonded symmetric O–H at around 3500 cm^{-1} is not discussed by the authors, but is likely due to some water molecules still present within the polymer matrix as the signal immediately rose from unaged to 90 days and remained at the same level even after 700 days. If it was the alcohol group present on the carboxylic acids, the signal would be not only stronger, but also closer to the C–H_2 signals [91]. We note that on the FTIR spectra of PA6 aged in hot dry air, this signal is not present.

As amides are broken into carboxylic acids and amine end groups, the carbonyl region assigned with the carboxylic acid group should rise in intensity. Figures 27–29 display the 1800 to 1650 cm^{-1} IR region of PA6 samples aged in deoxygenated water, dry air, and oxygenated water at 80 °C over time.

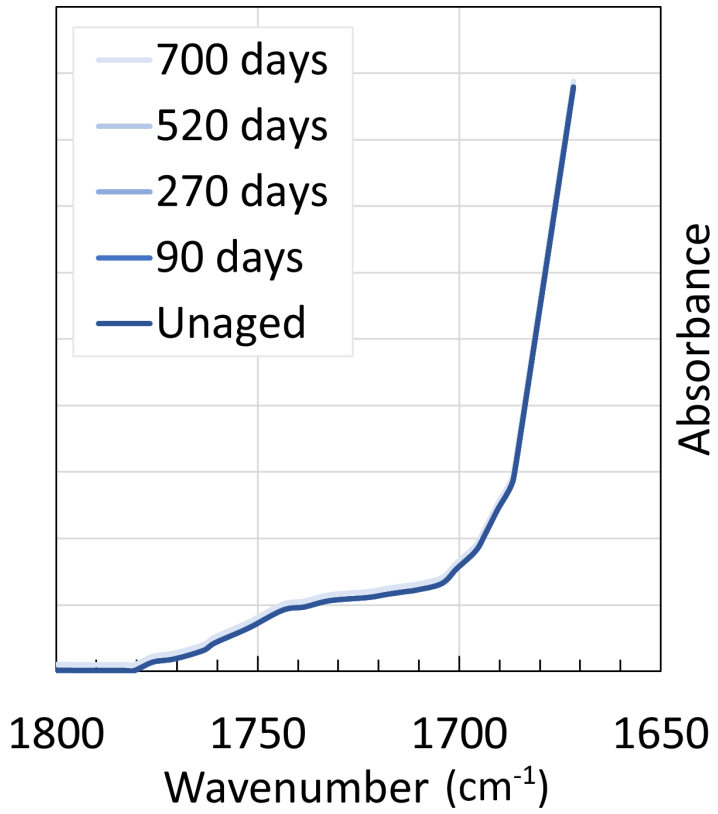

Figure 27. Infrared carbonyl region of PA6 aged in pure water at 80 °C. Data from [48].

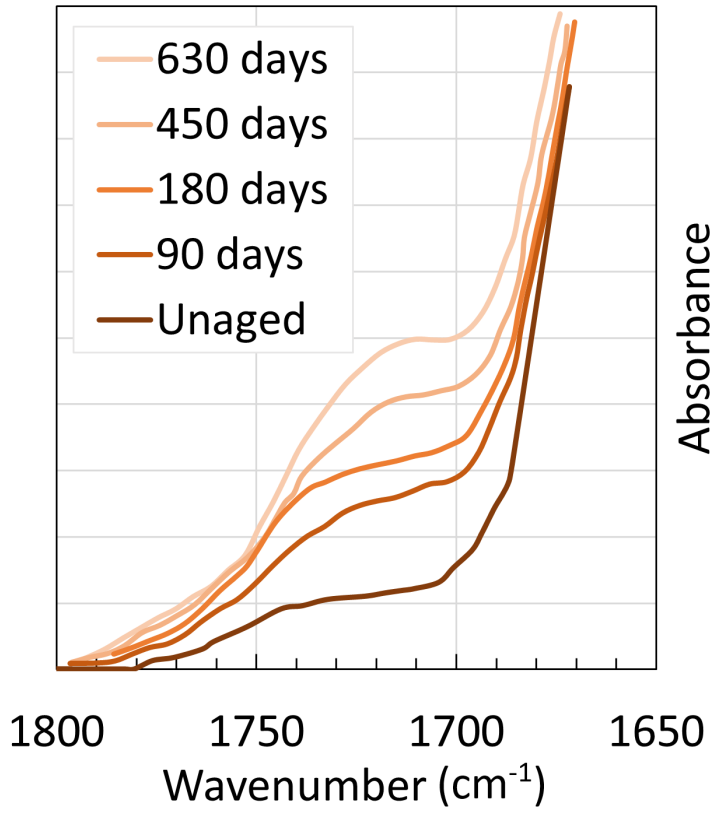

Figure 28. Infrared carbonyl region of PA6 aged in dry air at 80 °C. Data from [48].

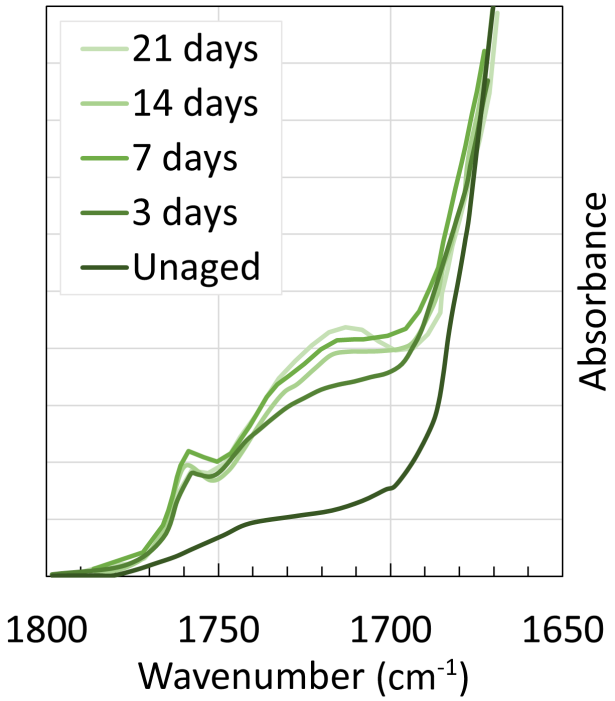

Figure 29. Infrared carbonyl region of PA6 aged in oxygenated water at 80 °C. Data from [48].

The amide IR signals lie at around 1630 and 1530 cm^{-1} and are seen in all three FTIR spectra in the article. A signal is detected at around 1730 cm^{-1} in samples aged in dry air and two new signals at 1760 and 1730 cm^{-1} for samples aged in oxygenated water, all while no signals are seen for samples aged in deoxygenated water even after 700 days of aging. Deshoulles et al. [48] assigned the signal at 1760 cm^{-1} to C=O of isolated carboxylic acids and 1730 cm^{-1} to C=O of imides. The formation of imides during oxidation of polyamides has been established before, notably by Gonçalves et al. [8]. Their work also included a full chemical pathway for PA66 degraded via hydrolysis and oxidation coupled together. They were able to detect the presence of imides formed at low temperatures ranging from 40 °C to 80 °C after only 160 hours of aging.

While the signal for imides is expected to not be present on the IR spectra of PA6 samples aged in deoxygenated water, the lack of signal from carboxylic acids is likely due to the extremely slow degradation rate of these samples. At 80 °C, pure hydrolysis is drastically slower. As mentioned in Section 2, PA6 aged in oxygenated water at the same temperature degraded 80 times faster than the ones aged in deoxygenated water when tracking the M_n. The M_n and X_c seen in Figure 2 from Section 2 and Figure 15 from Section 3 for that sample after 700 days are, respectively, high and low as opposed to other more degraded samples. In addition, equilibrium has not been reached, and probably neither was embrittlement as well. This is discussed in Section 5.3.

The authors also proved that the imide formed during thermal oxidation is easily hydrolyzed thereafter. Since hydrolysis starts at the carbon of the carbonyl group, due to its electropositive nature, the presence of two of them likely enhances the probability of occurrence. Nonetheless, when samples are left aging in hot dry air until equilibrium, and then left to age in hot deoxygenated water, the signal at 1730 cm^{-1} decreases, showcasing the consumption of the imide groups. The equilibrium reached in aging PAs in dry hot air is unique to thermal oxidation, and dissimilar to pure hydrolysis.

4.2. Polyamide 11

When comparing the FTIR spectra of PA11 and PA6, the main difference is the stronger C–H_2 signals in PA11 in relation to the other bands due to the longer aliphatic chain of the polymer. Hocker et al. [59] performed FTIR on their graphene oxide (GO)-reinforced

PA11 aged in deoxygenated water and investigated the ways in which they would impact the chromophores of the polymer. The FTIR spectra of unaged and aged PA11 without reinforcement are shown in Figure 30.

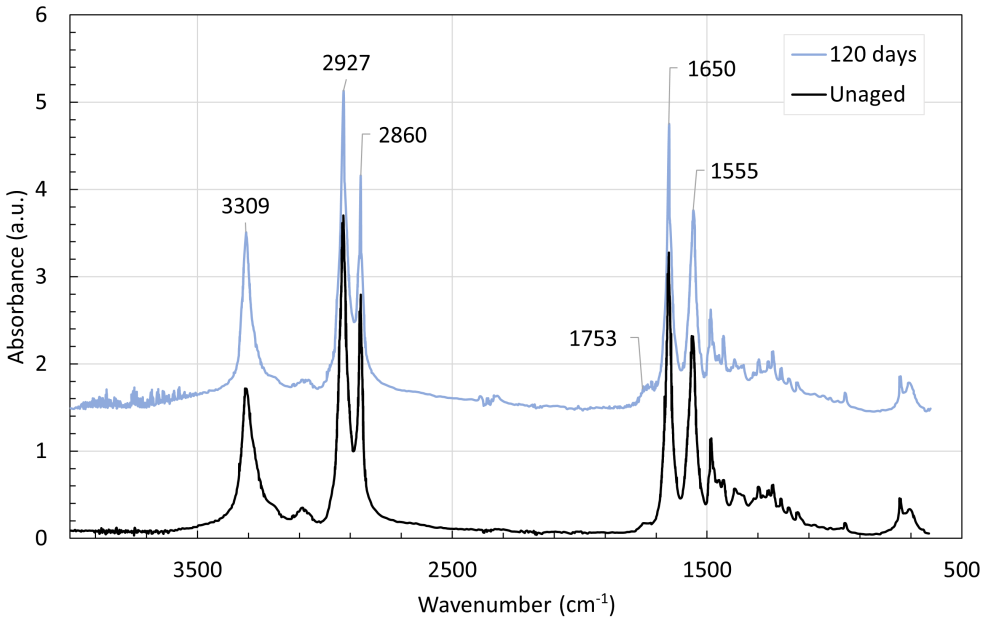

Figure 30. Infrared spectra of PA11 aged in deoxygenated hot water at 120 °C for 120 days. The signals of interest are labelled. Data from [59].

According to the authors, no major changes are observed when comparing the two spectra, even though, as shown in Figure 8 from Section 2, equilibrium seems to have been reached after 120 days of aging. We could argue that the 1700 to 1760 cm^{-1} region is rougher for the samples aged than the ones unaged, indicating that either imides or carboxylic acids are formed. The formation of imides would be illogical as the oxygen content in the water was controlled during aging. This may be solely coming from carboxylic acid group formation.

As stated earlier, the ability of certain functional groups to absorb infrared radiation is affected by crystallinity originating from the hydrogen bonds. Here, Hocker et al. [59] measured the half-height peak width of the amide III N–H stretch signal at 3309 cm^{-1}, which corresponds to the distribution of hydrogen bonded strength of the amide bond. It was shown that the width decreased from 54 to 34 ± 2 cm after aging, indicating a narrower distribution of hydrogen bonded strengths and hence a higher overall crystallinity content [92].

The presence of GO as reinforcement in PA11 showed a stronger signal at 1155 cm^{-1} than neat PA11. As this peak is assigned to the N–H stretch and O=C–N deformation, this suggests that the GOs were interacting with the N-H of the amide. This inhibits chain mobility, thereby slowing the rise in crystallinity, and then the degradation of the polymer.

Maïza et al. [57] also used FTIR to detect any changes in functional groups of their PA11. While they did remove any oxygen in the aging vessel, they stipulate that peroxides were formed during extrusion of their sample, which they used FTIR to confirm. Peroxides are products of oxidation, as hot molecular oxygen abstracts a hydrogen from the alpha carbon of the polyamide, leaving an alkyl radical at said carbon. The overall FTIR spectra are identical to the ones seen in Figure 30, with the exception of the carbonyl region from 1700 to 1760 cm^{-1}. Figure 31 shows the changes occurring in that region over different aging conditions.

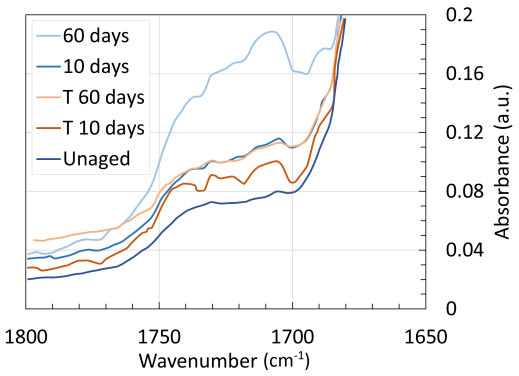

Figure 31. Infrared carbonyl region of PA6 aged in deoxygenated water and nitrogen gas (T) at 110 °C and pH 4. Data from [57].

PA11 were aged in deoxygenated water and nitrogen gas (T) for up to 60 days. No new carbonyl groups were formed when aging PA11 without air nor water, as expected, since no oxidation or hydrolysis can occur. A signal does appear for samples aged in deoxygenated water after 60 days at around 1720 cm^{-1}, which is likely corresponding to the formation of imides as also seen for PA6 aged with oxygen in Figures 28 and 29, thus proving the presence of oxidation products from the extrusion process. This example showcases the importance of controlling the oxygen environment of the PA during the entire time of the process.

5. Mechanical Properties

5.1. Polyamide 6

The fracture toughness of a 5 mm thick PA6/C immersed in hot deoxygenated water for up to 90 days was measured. The fracture tests were made from Arhant et al. [52] using an Instron testing with a load cell of 500 N at a speed of 1 mm/min. The samples were pre-cracked to only track the crack propagation. The fracture toughness, or critical strain energy release rate (G_{IC}), was determined empirically from the load and displacement of the material. For display, the stress–strain curves at 100 and 140 °C are shown in Figures 32 and 33. The changes in G_{IC} over time and temperature are depicted in Figure 34.

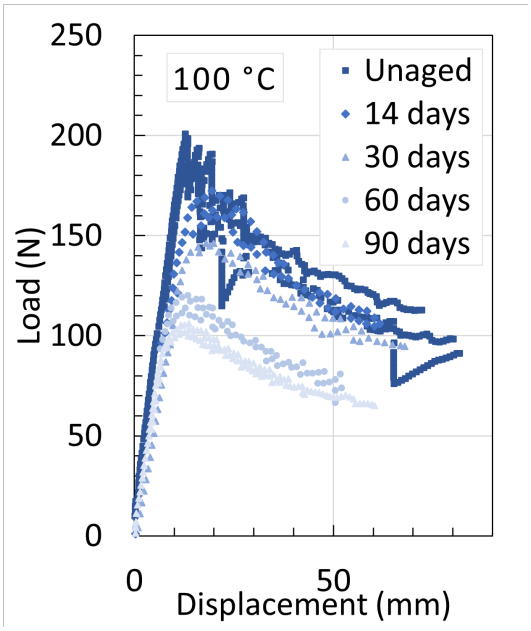

Figure 32. Stress–strain curves of PA6/C aged at 100 °C over time. Adapted with permission from ref. [52]. Copyright © 2021 Elsevier Ltd.

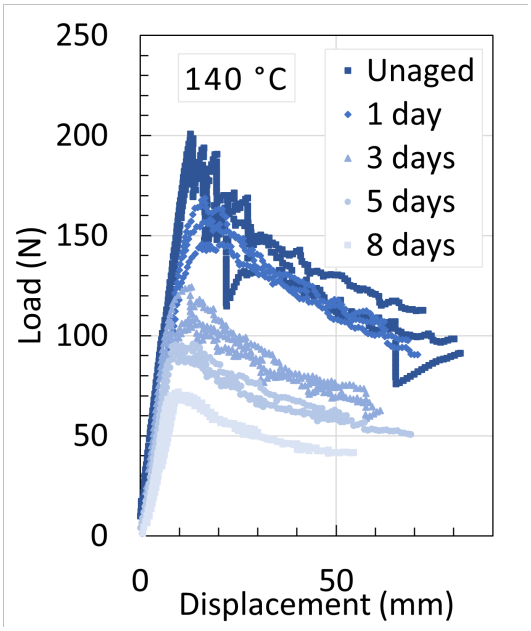

Figure 33. Stress-strain curves of PA6/C aged at 140 °C over time. Adapted with permission from ref. [52]. Copyright © 2021 Elsevier Ltd.

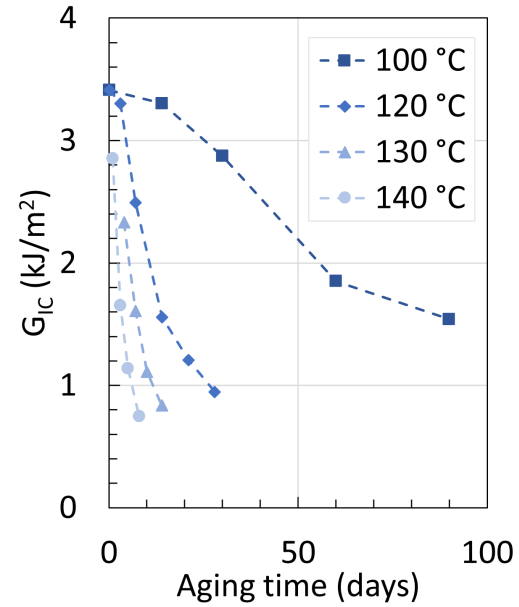

Figure 34. Changes in G_{IC} of PA6/C over time and temperature. Adapted with permission from ref. [52]. Copyright © 2021 Elsevier Ltd.

Fracture toughness decreases over time and does so drastically faster with increasing temperature. This is in correlation with the variations of molecular weight and crystallinity seen in the previous sections. The reduction in ultimate stresses for these PAs samples also aligns with the data from Bergeret et al. [63], where the ultimate stress of their PA66/30% GF fell by about 50% after aging at 120 °C for 200 hours (8.3 days).

Arhant et al. [53] also published, in the same year, another work regarding the aging of PA6/C in hot deoxygenated water. Using a similar methodology, the group focused on modeling fatigue crack growth behavior at various constant energy, or ΔG, as stated in their article. Figures 35 and 36 show the Hartman–Shijve representation of the fatigue crack growth of 5 mm thick PA6/C aged at 100 °C and 140 °C, respectively.

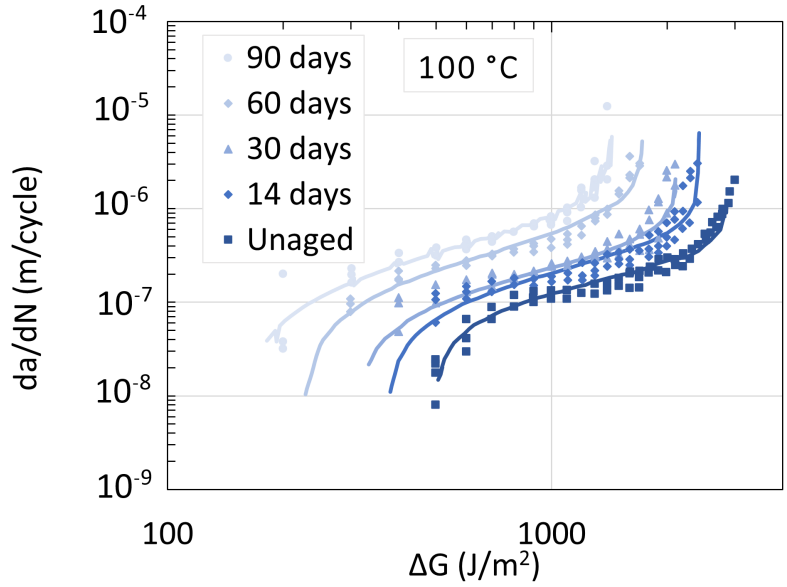

Figure 35. Plot of fatigue crack growth rate against ΔG over time at 100 °C with model fit. Data from [53].

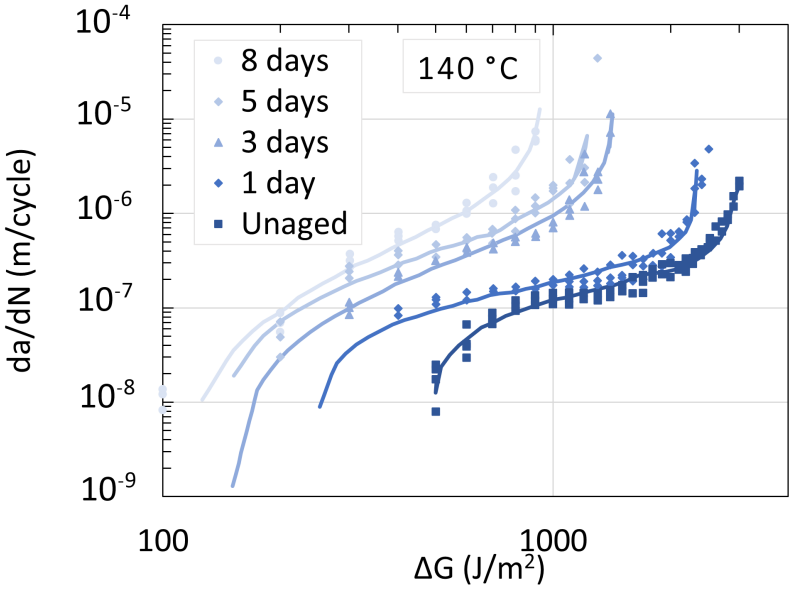

Figure 36. Plot of fatigue crack growth rate against ΔG over time at 140 °C with model fit. Data from [53].

Hydrolysis fastens the fatigue crack growth rate from 10^{-7} for unaged samples to 10^{-6} cm after 90 days at 100 °C and from 10^{-7} to 10^{-4} cm for aging samples at 140 °C at a set constant ΔG of 1000 J/m^2. When plotting their sigmoidal curves following the Hartman–Shijve representation, Arhant et al. [53] also fit their experimental data with a model that displayed an average R^2 of 0.9. An Arrhenius plot was constructed based solely on the fatigue crack growth rate, and an activation energy of 102 kJ/mol was found. The effect of degradation on the PA6/C was also readily observable using scanning electron microscopy (SEM) on fracture surfaces.

The strain at break and maximum stress were measured for 0.25 mm thick neat unstabilized PA6 aged under both pure hydrolysis and thermal oxidation separately. The data from Deshoulles et al. [55] are shown in Figures 37 and 38.

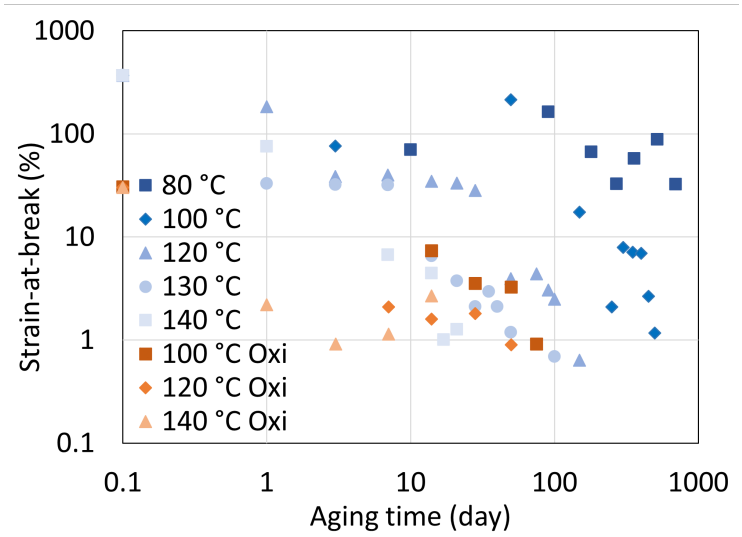

Figure 37. Strain at break of PA6 under pure hydrolysis or thermal oxidation over time and temperature. Data from [55].

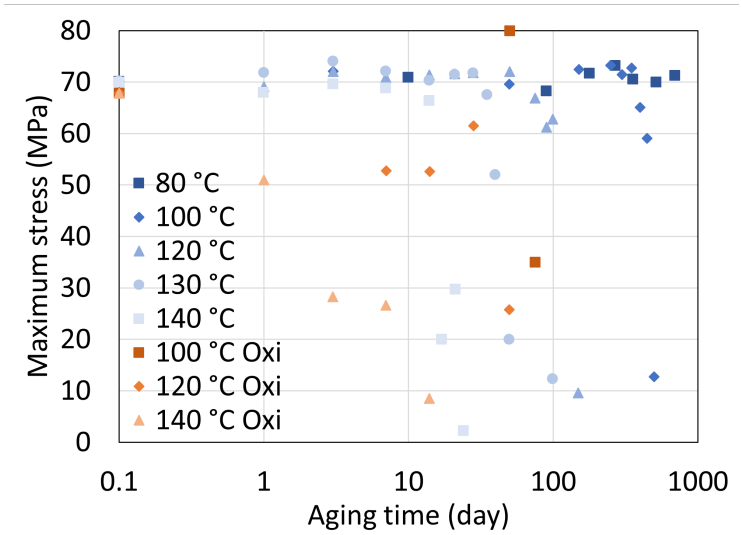

Figure 38. Maximum stress of PA6 under pure hydrolysis or thermal oxidation over time and temperature. Data from [55].

The strain at break decreases exponentially over time, and temperature rises from 300% to under 10% on average, while the maximum stress retains a plateau at around 70 MPa before significantly decreasing to 0 MPa for pure hydrolysis. At 80 °C and 100 °C, the decrease in strain at break is not as exponential as that for the higher temperatures. The drop seen in the maximal stress happens sooner for higher aging temperatures. For thermal oxidation, the strain at break and maximum stress reached similar values as those of pure hydrolysis, although in a shorter amount of time while at the same temperature and in a different context.

Similar behavior was measured from Bernstein et al. [65] when unreinforced PA66 was aged under a 100% humidity in argon or oxygen over time. The average tensile strength remaining of the PA66 straps was measured. This percentage dropped from 100% to 24% after 60 days when the sample was exposed to water vapor at a relative humidity of 100%, a temperature of 124 °C, and under argon atmosphere. When oxygen was introduced, the average fell to 18% after merely 18 days. The enhanced combined effect of hydrolysis and oxidation was also recorded for PA66. Strangely, aging PA66 straps in oxidation alone resulted in a slower rate of degradation. The average tensile strength remaining fell from

100% to 22% after 395 days. This result does not align with the fact that oxidation leads to a faster degradation, which may indicate that their aging process under argon was contaminated with water.

5.2. Polyamide 11

Samples of 0.5 mm thick heat and light stabilized with 12.5 wt% N-butyl benzenesulfonamide (BBSA) plasticizer PA11 were aged under pure hydrolysis condition, and the tensile strength was measured over time. This was performed by Mazan et al. [60,93,94] to create a multiscale model that allows the prediction of the polymer's mechanical properties and morphological parameters. The stress–strain curve is shown in Figure 39. For comparison, the tensile strength measurements from Maïza et al. [57], performed on a 1.5–2 mm thick PA11 containing BBSA and 0.8 wt% antioxidant under pure hydrolysis and anaerobic thermal aging conditions separately at 110 °C and pH 4, are shown in Figure 40.

For both graphs, at constant temperature, the strain at break occurs at lower strain with increasing aging time. This is in accordance with Figure 37. The maximum stress also seems constant throughout the different aging time, indicating that perhaps the degradation stage that induced the drop seen in Figure 38 has not occurred yet.

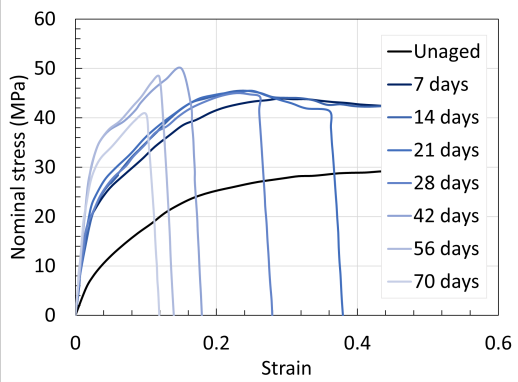

Figure 39. The stress–strain curve of PA11 under pure hydrolysis over time at 120 °C. The unit of strain is unspecified. Data from [60].

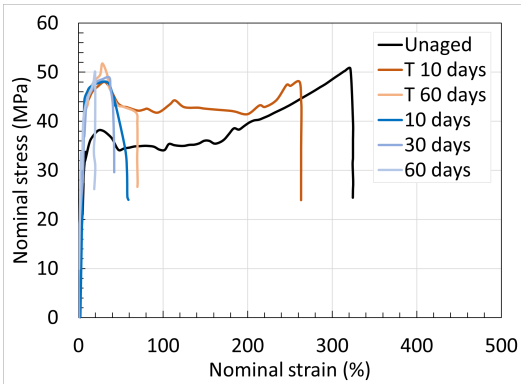

Figure 40. The stress–strain curve of PA11 under pure hydrolysis and anaerobic thermal (T) aging over time at 110 °C. Data from [57].

The Young's modulus also increases as aging happens. Not only that, but it increases fast from unaged to the first 10 days for both graphs. This rapid change is expected to originate from the early loss of plasticizer. Mazan et al. [60] used thermogravimetric analysis (TGA) to determine the extractable content of plasticizer in PA11. They found that this amount drops from 16% to 4–2% within the first 7 days depending on the temperature. It then stagnates into a plateau. The known big early drop in M_w was also expected to decrease the tensile strength and modulus, but this was not seen. According to the authors,

the loss of plasticizer is enough to hide the mechanical effect caused by the initial drop in M_w. Indeed, both authors claim that the first yield stress originates from the plasticization of the crystals and sliding of chains in the amorphous phase, while the increased second yield stress is due to a destruction of such crystals, resulting in a higher degree of crystallinity within the PA11 matrix.

Lastly, both authors noted a change in the mechanical behavior between 30 and 60 days. In that range, a large increase in the first yield stress was seen, and Maïza et al. [57] attributed it to the high degree of crystallinity. As the crystals grow larger during aging, they require additional energy for breakage or, i.e., to reach the second yield stress.

5.3. Determination of Embrittlement

Polymer embrittlement is a property threshold in which a polymer transitions from harboring a ductile property to a brittle one. The fragmentation of these brittle polymers into secondary plastics in the ocean is also a result of such phenomenon, often caused by chemical aging [95]. The transition is complex and dependent on the nature of the polymer. Hence, many authors aim to determine the point of embrittlement to model the lifetime of their polymer of interest. This is not exclusive to pure hydrolysis.

Arhant et al. [52,53] used fracture toughness and crack propagation rate as the tracking mechanical property embrittlement of their PA6/C. This was achieved by observing the changes in M_n against these mechanical parameters. Figure 41 and Figure 42 display the impact that low M_n has on G_{IC} and crack propagation rate, respectively.

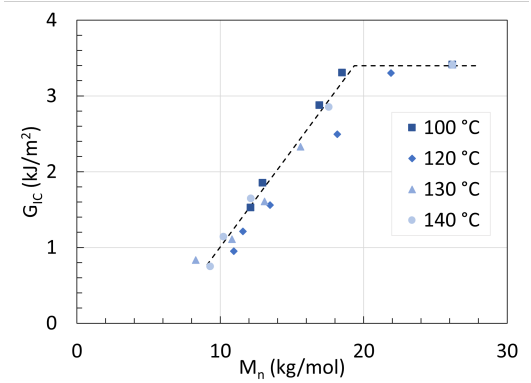

Figure 41. Fracture toughness of PA6/C aged at varying temperature against M_n with trendline. Adapted with permission from ref. [52]. Copyright © 2021 Elsevier Ltd.

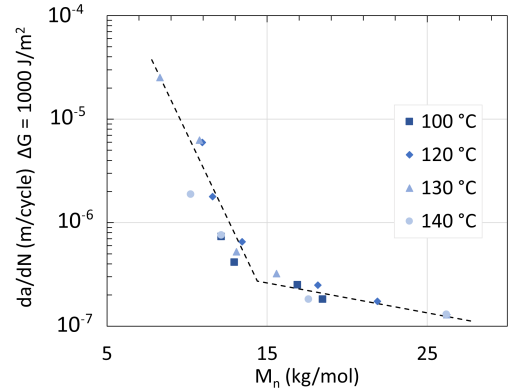

Figure 42. Crack propagation rate of PA6/C aged at varying temperature against M_n with trendline. Adapted with permission from ref. [53]. Copyright © 2022 Elsevier Ltd.

The decrease in G_{IC} under Mode I static loading began when M_n = 18 kg/mol, regardless of temperature. According to the authors, this behavior was seen before in earlier work related to neat polypropylene [96]. This value is also close to that of other semi-crystalline

polymers like PET or PA11. To Arhant et al. [52], this similarity proves the impact of fibers being negligible on degradation for the modeling of embrittlement. However, following the previous data presented in this review, reinforcement does play a role in water absorption. While reinforcement may not impact the point of embrittlement, it impacs the hydrolysis degradation rate. Finally, an Arrhenius plot of fracture toughness, mass loss, X_c, and M_n offered an activation energy of 105, 105, 113, and 115 kJ/mol with $R^2 > 0.99$, indicating that the same mechanism is impacting these four parameters.

A similar behavior was seen from the variations of crack propagation rate under Mode I fatigue loading conditions, though the linearity of the measurements stopped at around M_n = 15 kg/mol instead. The authors described this new threshold to be more accurate than the one using fracture toughness under static loading. According to them, when the length of the polymer chain is higher than the threshold, a crack can be spanned and an additional increase in M_n cannot be measured. That is to say, after 15 kg/mol, the entanglement network between polymer chains is no longer strong enough to hinder crack propagation. PA6/C is seemingly more sensitive to cyclic loading than quasi static, which is partially thought to origin from the polymer network being unraveled under such loading. Regardless of the aging temperature, hydrolysis fastened the crack propagation rate by a decade.

Work by Olufsen et al. [54] aimed at understanding the effect of loading conditions on embrittlement and highlighted their importance. In their study, PA11 with and without 6% BBSA was aged in pH 3 butanoic acid at 120 °C for accelerated aging. Instead of GPC, they used a viscometer to measure the correct inherent viscosity (CIV) of the PA11 and performed tensile tests on them. The aimed CIV levels were predetermined from the literature to be 0.7 and 1.2 dL/g. The authors showed that experimental conditions such as temperature of tensile tests, nominal strain rate, notch radius, CIV levels aimed, and initial plasticizer content yielded different responses from the test specimens aged in deoxygenated hot water. Three types of responses were considered: brittle failure with no apparent plasticity, ductile failure at necking without cold drawing, and ductile failure after cold drawing. A change from ductile to brittle failure was possible with a constant CIV level and plasticizer content. From these parameters, the resulting secant modulus (E_{sec}), yield stress (σ_{20}), hardening modulus (H), and failure strain (ε_f) were tracked. The main conditions required from the experimental variables to express a high or low response parameter are shown in Table 1.

Table 1. The principal effects of experimental variable upon the physical response parameters from tensile testing of PA11. The gray background represents a lack of data/correlation. Data from [54].

	Temperature	**Strain Rate**	**Notch Radius**	**CIV**	**Plasticizer**
High E_{sec}	Low	High	-	-	Low
High σ_{20}	-	High	High	Low	Low
Low H	-	High	High	-	-
Low ε_f	-	-	-	Low	-

Overall, any parameters increasing the level of stress in the material specimens yielded a brittle failure response from the tensile tests. The authors also found that the nominal strain at failure may be the issue of cold drawing rather than the material's degradation. Apart from these details, the paper did not investigate embrittlement further.

The core of the work from Deshoulles et al. [55] was the investigation of the origin of embrittlement. The correlation between strain at break and maximal stress against M_n of neat PA6 is shown in Figure 43 for strain at break and Figure 44 for maximum stress together with other published data [97–100].

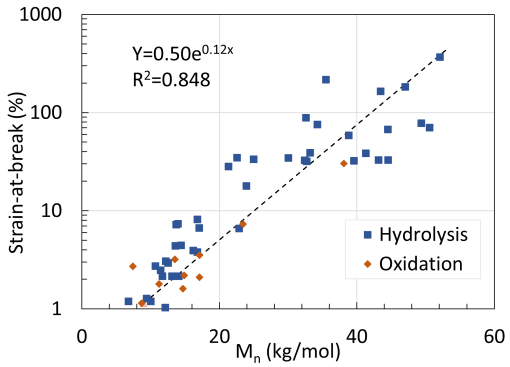

Figure 43. Strain at break against M_n under pure hydrolysis and oxidation with linear correlation for neat PA6. Adapted with permission from ref. [55]. Copyright © 2021 Elsevier Ltd.

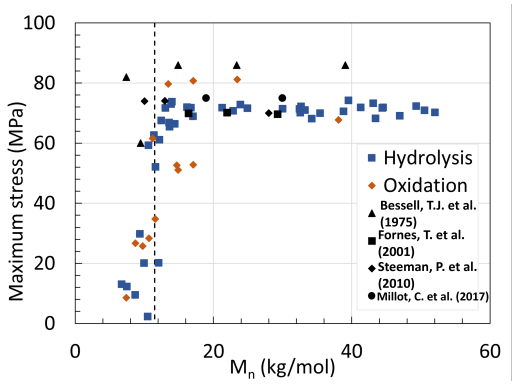

Figure 44. Maximum stress against M_n under pure hydrolysis and oxidation for neat PA6. The dotted line showcases the M_n at which the maximum stress drops. Data from [55], the triangle, square, diamond, and circle symbols are from the following sources respectively [97,98,100].

When the M_n of PA6 drops due to chain scission, the strain at break and maximum stress display similar values regardless of the conditions. The strain at break decreases in a logarithmic way over M_n, while the maximum stress remains at around 70 MPa before dropping drastically after around 15 kg/mol as written by the authors. This correlation proves that embrittlement can be tracked and estimated by solely tracking the M_n of PA6 when degraded either through hydrolysis or oxidation.

Deshoulles et al. [55] linked the decrease in strain at break to the presence of tie molecules between amorphous and crystalline phases of the PA6 matrix. Following a probability equation based on the work from Huang and Brown [101], with some adjustments from Seguela [102], the theoretical probability of tie molecules can be calculated. A relatively scattered correlation with a R^2 of 0.661 was reached for hydrolysis and oxidation combined when plotting the strain at break with the probability of tie molecules present. As the probability lowers, so does the strain at break. The high scattering is said to originate from the complexity of measuring the strain at break of an aged PA6 sample. This correlation is not applicable for maximum stress; however, the average number of entanglements (q) based on the literature and gel permeation chromatography (GPC) data can be used instead. With this, the authors found that when $q < 5$, the maximum stress drops regardless of the degradation mechanisms. Hence, an average of five entanglements would, in this scenario, be one of the criteria threshold for embrittlement. Deshoulles et al. [55] also listed other works showcasing a similar value for other semi-crystalline polymers like PA11 and PET degraded through oxidation or hydrolysis [13,103].

Apart from M_n, X_c was also plotted against the two mechanical properties; the corresponding graphs are shown in Figures 45 and 46.

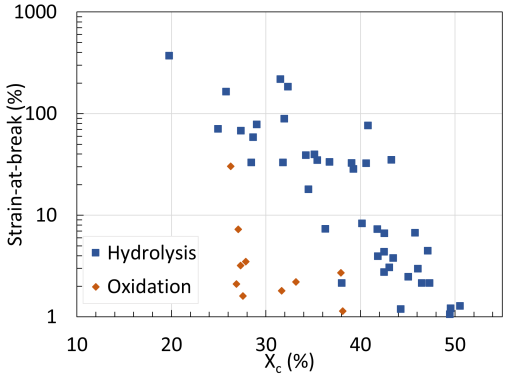

Figure 45. Strain at break against X_c under pure hydrolysis and oxidation condition with linear correlation for neat PA6. Adapted with permission from ref. [55]. Copyright © 2021 Elsevier Ltd.

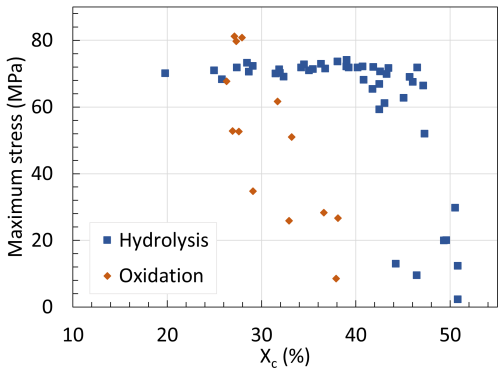

Figure 46. Maximum stress against X_c under pure hydrolysis and oxidation condition for neat PA6. Adapted with permission from ref. [55]. Copyright © 2021 Elsevier Ltd.

At first, we can notice the X_c of PA6 does not harbor the same mechanical properties depending on the degradation mechanisms. This was to be expected. As mentioned in the previous section, during hydrolysis, water forms hydrogen bonds with the PA6 matrix and induces plasticization, a physical process in which the polymer not only swells, but also increases in crystallinity. This is then followed by chemi-crystallization. The correlation between strain at break and X_c remains linear, but only when separating the data from pure hydrolysis and oxidation. The drop in maximal stress is only observable for the samples aged in deoxygenated water. Embrittlement seems to happen when $X_c > 45\%$, as shown from both the strain at break and maximum stress. Tracking X_c is hence only usable for PAs aged in deoxygenated hot water. Olufsen et al. [54] also indicated that crystallinity can be used as an indicator for embrittlement.

Deshoulles et al. [55] also tracked the amorphous layer thickness (*la*). This parameter can be calculated using wide-angle x-ray spectroscopy (WAXS) and GPC data. *la* is thus linked to the morphology of crystal phases and molecular weight. The data for *la* are showing similar trends as the ones for M_n. If $la < 5$ nm, PA6 harbors a brittle behavior. The authors make the claim that the relationship between *la*, M_n and M_w is also applicable as the PDI does not change during aging. However, this is only true for pure hydrolysis. As seen in Section 2, the PDI increases for samples aged in hot dry air. Regardless, their work shows clear indications that M_n and *la* can be used to track embrittlement for both hydrolysis and oxidation mechanisms. X_c can also be used, although only for sample degraded via pure hydrolysis. M_n correlates with the one found by Arhant et al. [53] from the crack propagation rate data.

The tensile strength of the PA11 aged by Costa et al. [51] in aqueous cooling fluids containing acetate and propionate ions with a pH of 5.5 was assessed. As expected, the strain at break decreased over time from around 350% to 25% after 109 days at 120 °C in

a relatively exponential way. The authors tracked the CIV as well and discovered that a plateau of 1.0 dL/g was reached after 40 days of aging, all while the strain at break kept decreasing after such aging time. A TGA measurement showed that the amount of plasticizer decreased similarly to the strain at break after reaching the CIV plateau aging time. This indicates that rather than shortening the length of the polymer chains, the PA11 matrix undergoes conformational changes due to the loss of plasticizer.

The already mentioned work from Hocker et al. [58] aimed at aging PA11 with different organic acid solutions to accelerate hydrolysis. In this way, they investigated the individual importance of using molecular weights and crystallinity. The authors used tensile test measurements and defined the polymer to harbor brittle behavior once the sample reached an ultimate strain of less than 100%. Their GPC and DSC data combined with their tensile tests results are shown in Figures 47 and 48, respectively.

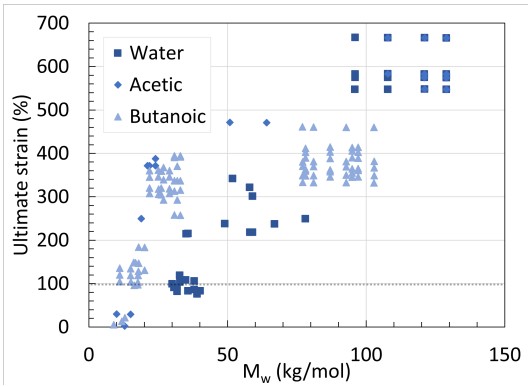

Figure 47. Correlation between ultimate strain and M_w of PA11 aged in water and organic acids. Adapted with permission from ref. [58]. Copyright © 2018 Elsevier Ltd.

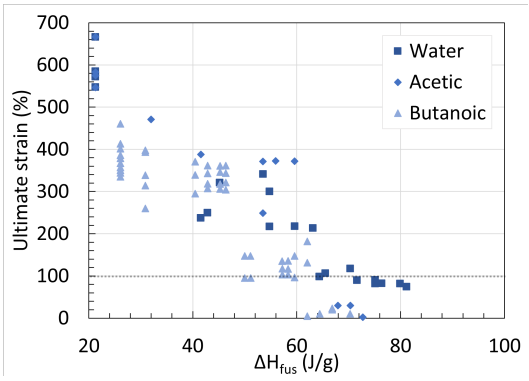

Figure 48. Correlation between ultimate strain and melting enthalpy (ΔH_{fus}) of PA11 aged in water and organic acids. Adapted with permission from ref. [58], Copyright ©2018 Elsevier Ltd.

When looking at Figure 47, a M_w of PA11 samples aged in water between 30 to 40 kg/mol corresponded to an ultimate strain of 100%, while the ones aged in butanoic acid and acetic acid did not reach embrittlement at that range and possessed an ultimate strain of about 350%. This is despite the fact that the samples aged in both solutions were in a more advanced degradation state than the ones for water. On the contrary, Figure 48 shows that the correlation between ΔH_{fus} and ultimate strain follows a linear trend, regardless of the organic acid used. This means that crystallinity is a more accurate determinant of embrittlement than chain length. For this material, when $\Delta H_{fus} > 67$ J/g or $X_c > 35\%$, if $\Delta H_{fus} = 189$ J/g for 100% crystalline PA11, embrittlement is expected regardless of molecular weight. Using a ΔH_{fus} of 226 J/g, this X_c threshold was equal to 30%. This is either way lower in value than the 45% found for PA6. This perhaps means that PA6 can hold its ductile ability better than PA11 despite high crystallinity. The lower water

absorption ability of PA11 and the presence of BBSA as plasticizer are both likely dropping the crystallinity of X_c in value.

There are some side notes. The authors stipulate that embrittlement has its transition onset starting at around 55–60 J/g for butanoic acid, implying that the range is relatively large. However, this can be explained by the presence of small organic acid molecules, decreasing the ΔH_{fus} at embrittlement. These molecules diffuse themselves into the matrix depending on concentration, temperature, and solubility. The presence of BBSA is known to disrupt and reduce crystallinity, which also impacts ΔH_{fus} at embrittlement. Hocker et al. [58] speculated that the ultimate strain would decrease by about 20%.

Equilibrium was reached for M_w due to recombination for PA11 aged in water after 50 days as seen in Figure 10. At that time, ΔH_{fus} does not reach equilibrium, but rather rises from 67 to 81 J/g after 240 days of aging, showcased in Figure 25. This increase is originating from thermal annealing according to the authors.

The shortening of chain length seen from the reduction in M_w and subsequent rise in chain mobility lead to chemi-crystallization which increased X_c. In other words, the two parameters are inter-connected with one another, hence their similarity in behavior. However, according to Hocker et al. [58], for the determination of embrittlement, chain scission acts more as the enabler for the formation of hydrogen bonds. These hydrogen bonds are responsible for the brittle behavior of the material.

6. Mechanism Overview

Before immersion in water, the matrix of polyamide (PA) materials consists of long aliphatic chains containing amide groups in the middle as well as carboxylic acid and amine end groups, depending on the type of PA. These groups form hydrogen bonds with themselves, which makes up the α-crystalline structure of the polymer. Areas lacking such dipole–dipole interactions are β-amorphous.

Immediately after immersion, the polymer undergoes plasticization, resulting in a fast increase in crystallinity ratio, a decrease in molecular weight and mechanical strength. The water molecules diffuse through the matrix, swelling and expanding the material. The kinetics of diffusion are discussed in detail in the review written by Venoor et al. [21]. When the matrix is saturated with water, the water molecules start creating and inserting new hydrogen bonds between the polar groups of the amorphous areas of the polymer. This causes a transition from a β-amorphous to a monoclinic α-crystalline phase which is only possible when aging PAs in water. The presence of water induces water-assisted hydrolysis on the amide middle groups, provoking chain scissions randomly over the polymer chains. From a chemical point of view, two molecules of water react with the electropositive carbon of the amide carbonyl in a concerted way. Following the Grotthuss mechanism, a proton simultaneously jumps from the then-formed hydronium cation, leading to the formation of a primary amine and a carboxylic acid group [59]. The basic reaction mechanism is shown in Figure 49.

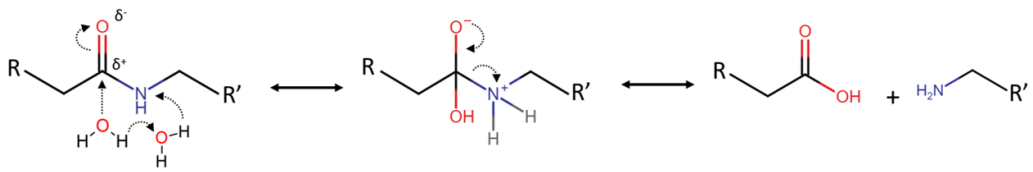

Figure 49. Reaction mechanism of water-assisted hydrolysis of amide groups.

After plasticization, the material undergoes chemi-crystallization, a process in which the shorter polymer chains obtain higher mobility within the matrix which allows them reorganization into new crystallites. This is governed by the new hydrogen bonds formed between end groups and bound water. Ultimately, hydrolysis reaches chemical equilibrium where condensation rivals thermodynamically. This is shown by a stalemate in the rise of crystallinity, a decrease in molecular weight, and a decrease in mechanical strength over time. Depending on the conditions, it is likely that the PA transitioned from harboring

a ductile mechanical property to a brittle one, i.e., reached embrittlement. At this point, the concentration of tie molecules between crystalline and amorphous phases as well as the number of entanglements reaches a critical threshold that results in a drastic drop in maximal stress of the material. For clarity, an illustration of changes occurring in the PA matrix over aging time is shown in Figure 50.

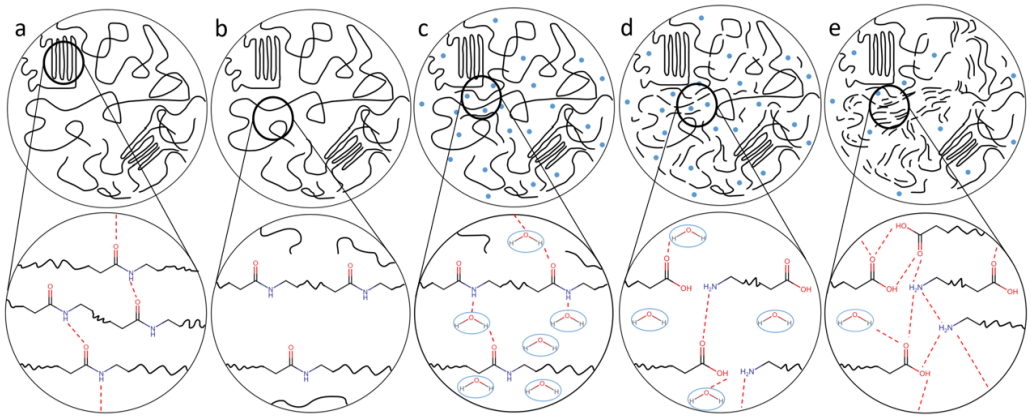

Figure 50. Illustration of the changes occurring within the PA matrix when aging in deoxygenated water. (**a**) Crystalline phase before immersion in water, (**b**) amorphous region before immersion, (**c**) plasticization with free and hydrogen bound water, (**d**) chain scission due to hydrolysis, (**e**) chemi-crystallization. The blue circles and red dotted lines represent water molecules and hydrogen bonds.

7. Conclusions and Perspective

To the best of our knowledge, most if not all the research relevant to the degradation understanding of polyamide (PA) under pure hydrolysis is compiled in this review. When aged in hot deoxygenated water, PA degrades through hydrolysis, decreasing its molecular weight, mechanical strength, and rising the crystallinity ratio in a logarithmic fashion over time. Increasing the temperature enhances this trend to reach the plateau faster, but can also further said plateau to reach more extreme levels. The kinetics of degradation and the changes in the molecular structure with PAs degraded under hydrolysis are also contrasted with those degraded under pure oxidation and hydrothermal oxidation. It is shown that both molecular weight and mechanical strength lessens the slowest when aging PA in deoxygenated water. The crystallinity ratio rises faster under pure hydrolysis than oxidation. The evidence of oxidation is also monitored using infrared spectroscopy by tracking the signals for imide groups.

The ductile to brittle transition or embrittlement is found to be traceable by crystallinity ratio. Molecular weight can also be used, but less so for the case of hydrolysis purely. An estimation on the molecular weight at the point of embrittlement is conducted in the cited work.

Analyzing each article also unravels gaps in the research. The question of embrittlement and which parameter to trust remains to be discussed and could be further researched by investigating the crystalline properties of PA6, PA66, and other PAs. Many factors impact the degradation of PAs in water, some more than others. Ultimately, if either crystallinity or molecular weight is found to be the most trustworthy parameter for other PAs, a model can be constructed along with all the factors listed in this review that impacts it. Models based on water absorption, water diffusion, kinetics, and more already exist, but often remain limited to the singular context in which they are made from. This review serves as a tool to glance at the work conducted on the matter and the many conclusions drawn from the data. The many graphs shown here can be used as reference for future novel research.

Author Contributions: Conceptualization, M.M.B. and J.d.C.C.; methodology, M.M.B.; validation, A.H.H.; investigation, M.M.B.; writing—original draft preparation, M.M.B.; writing—review and editing, A.H.H., A.D.D. and J.d.C.C.; visualization, M.M.B.; supervision, A.H.H., A.D.D. and J.d.C.C.; project administration, J.d.C.C.; funding acquisition, J.d.C.C. All authors have read and agreed to the published version of the manuscript.

Funding: This research was funded by Innovationsfonden (Innovation Fund Denmark), grant number 9091-00010B.

Data Availability Statement: Not applicable.

Conflicts of Interest: The authors declare no conflict of interest.

Abbreviations

The following abbreviations are used in this manuscript:

PA	Polyamide
GPC	Gel permeation chromatography
C	Carbon fiber
PDI	Polydispersity index
FTIR	Fourier-transform infrared
BBSA	N-butylbenzenesulfanomide
GO	Graphene oxide
DSC	Differential scanning calorimetry
XRD	X-ray diffraction
NMR	Nuclear magnetic resonance
SEM	Scanning electron microscopy
TGA	Thermogravimetric analysis
CIV	Correct inherent viscosity
WAXS	Wide-angle x-ray spectroscopy

References

1. Romão, W.; Castro, E.R.; Filho, E.A.S.; Guimarães, R.; Silva, A.L.N.; Teixeira, S.; Paoli, M.; Sena, G.L. Ageing of polyamide 11 used in the manufacture of flexible piping. *J. Appl. Polym. Sci.* **2009**, *114*, 1777–1783. https://doi.org/10.1002/APP.30793.
2. El-Mazry, C.; Correc, O.; Colin, X. A new kinetic model for predicting polyamide 6-6 hydrolysis and its mechanical embrittlement. *Polym. Degrad. Stab.* **2012**, *97*, 1049–1059. https://doi.org/10.1016/J.POLYMDEGRADSTAB.2012.03.003.
3. Shakiba, M.; Rezvani Ghomi, E.; Khosravi, F.; Jouybar, S.; Bigham, A.; Zare, M.; Abdouss, M.; Moaref, R.; Ramakrishna, S. Nylon—A material introduction and overview for biomedical applications. *Polym. Adv. Technol.* **2021**, *32*, 3368–3383, https://doi.org/10.1002/pat.5372.
4. Zhang, Y.; Wang, C.; Yi, Y.; Wang, W.; Yang, J. Synthesis and Properties of Polyamide 6 Random Copolymers Containing an Aromatic Imide Structure. *Polymers* **2023**, *15*, 2812. https://doi.org/10.3390/polym15132812.
5. Shamey, R.; Sinha, K. A review of degradation of nylon 6. 6 as a result of exposure to environmental conditions. *Color. Technol.* **2003**, *33*, 93–107. https://doi.org/10.1111/J.1478-4408.2003.TB00147.X.
6. Varghese, M.; Grinstaff, M.W. Beyond nylon 6: Polyamides via ring opening polymerization of designer lactam monomers for biomedical applications. *Chem. Soc. Rev.* **2022**, *51*, 8258–8275. https://doi.org/10.1039/D1CS00930C.
7. Grigg, M.N. Thermo-Oxidative Degradation of Polyamide 6. Ph.D. Thesis, School of Physical and Chemical Sciences Queensland University of Technology: Brisbane, Australia, 2006.
8. Gonçalves, E.S.; Poulsen, L.; Ogilby, P.R. Mechanism of the temperature-dependent degradation of polyamide 66 films exposed to water. *Polym. Degrad. Stab.* **2007**, *92*, 1977–1985. https://doi.org/10.1016/J.POLYMDEGRADSTAB.2007.08.007.
9. Holland, B.J.; Hay, J.N. Thermal degradation of nylon polymers. *Polym. Int.* **2000**, *49*, 943–948. https://doi.org/10.1002/1097-0126(200009)49:9<943::AID-PI400>3.0.CO;2-5.
10. Ullah, I.; Gul, T.; Ali, M.; Khan, I.; Khan, W.; Asghar, H.; Saeed, K. Preparation, Analysis and UV-Accelerated Photocatalytic Degradation of Pesticide Over Mg Doped ZnO/Nylon 6,6/PMMA Ternary Blend. *J. Inorg. Organomet. Polym. Mater.* **2023**, *33*, 3441–3453. https://doi.org/10.1007/s10904-023-02767-w.
11. Gröning, M.; Hakkarainen, M. Headspace solid-phase microextraction–a tool for new insights into the long-term thermo-oxidation mechanism of polyamide 6.6. *J. Chromatogr. A* **2001**, *932*, 1–11. https://doi.org/10.1016/S0021-9673(01)01230-4.
12. Vasanthan, N.; Murthy, N.; Bray, R. Investigation of Brill transition in nylon 6 and nylon 6,6 by infrared spectroscopy. *Macromolecules* **1998**, *31*, 8433–8435. https://doi.org/10.1021/MA980935O.

13. Okamba-Diogo, O.; Richaud, E.; Verdu, J.; Fernagut, F.; Guilment, J.; Fayolle, B. Molecular and macromolecular structure changes in polyamide 11 during thermal oxidation-Kinetic modeling. *Polym. Degrad. Stab.* **2014**, *108*, 123–132. https://doi.org/10.1016/J.POLYMDEGRADSTAB.2014.05.028.
14. Krejsa, M.; Udipi, K.; Middleton, J. NMR Analysis of UV- and Heat-Aged Nylon-6,6. *Macromolecules* **1997**, *30*, 4695–4703. https://doi.org/10.1021/MA9702051.
15. Sanders, B.; Cant, E.; Amel, H.; Jenkins, M. The Effect of Physical Aging and Degradation on the Re-Use of Polyamide 12 in Powder Bed Fusion. *Polymers* **2022**, *14*, 2682. https://doi.org/10.3390/polym14132682.
16. Moore, R. The photochemical degradation of polyamides and related model N-alkylamides. *Polymer* **1963**, *4*, 493–513. https://doi.org/10.1016/0032-3861(63)90062-4.
17. Levchik, S.; Weil, E.; Lewin, M. Thermal decomposition of aliphatic nylons. *Polym. Int.* **1999**, *48*, 532–557. https://doi.org/10.1002/(SICI)1097-0126(199907)48:7<532::AID-PI214>3.0.CO;2-R.
18. Mazry, C.E.; Hassine, M.B.; Correc, O.; Colin, X. Thermal oxidation kinetics of additive free polyamide 6-6. *Polym. Degrad. Stab.* **2013**, *98*, 22–36. https://doi.org/10.1016/J.POLYMDEGRADSTAB.2012.11.002.
19. Forsström, D.; Terselius, B. Thermo oxidative stability of polyamide 6 films. I. Mechanical and chemical characterisation. *Polym. Degrad. Stab.* **2000**, *67*, 69–78. https://doi.org/10.1016/S0141-3910(99)00122-6.
20. Thanki, P.N.; Singh, R.P. Progress in the Area of Degradation and Stabilization of Nylon 66. *J. Macromol. Sci.-Rev. in Macromol. Chem. Phys.* **1998**, *38*, 595–614. https://doi.org/10.1080/15583729808546033.
21. Venoor, V.; Park, J.H.; Kazmer, D.; Sobkowicz, M.J. Understanding the Effect of Water in Polyamides: A Review. *Polym. Rev.* **2021**, *61*, 598–645. https://doi.org/10.1080/15583724.2020.1855196.
22. Lottier, S.; Tencé-Girault, S.; Gervat, L.; Saintier, N.; Miquelard-Garnier, G.; Fayolle, B. Effect of chemical ageing on fatigue life of short glass fiber-reinforced Polyamide 6,6. *Polym. Degrad. Stab.* **2023**, *208*, 110244. https://doi.org/10.1016/j.polymdegradstab.2022.110244.
23. He, X.; Xiao, B.; Cai, G.; Takahashi, J. Morphological, physicochemical, and flexural characterization of carbon fiber paper–reinforced polyamide 6 for long-term application in aqueous environments. *J. Polym. Res.* **2021**, *28*, 362. https://doi.org/10.1007/s10965-021-02730-8.
24. Bäckström, E.; Odelius, K.; Hakkarainen, M. Microwave Assisted Selective Hydrolysis of Polyamides from Multicomponent Carpet Waste. *Glob. Challenges* **2021**, *5*, 2000119. https://doi.org/10.1002/GCH2.202000119.
25. Harrass, K.; Mauer, S.; Tsekov, R. Resistance of glass fiber reinforced polyamide 6.6 materials to automotive cooling fluids: An analytical method for lifetime prediction. *Polym. Int.* **2021**, *71*, 724–733. https://doi.org/10.1002/PI.6323.
26. Zhang, C.; Liu, C.; Zhao, H.; Hu, W.; Liu, G.; Zhao, Y.; Dong, X.; Wang, K.; Zhang, J.; Li, X.; et al. Effect of nanoparticle and glass fiber on the hydrothermal aging of polyamide 6. *J. Appl. Polym. Sci.* **2020**, *137*, 49585. https://doi.org/10.1002/APP.49585.
27. Češarek, U.; Pahovnik, D.; Žagar, E. Chemical Recycling of Aliphatic Polyamides by Microwave-Assisted Hydrolysis for Efficient Monomer Recovery. *ACS Sustain. Chem. Eng.* **2020**, *8*, 16274–16282. https://doi.org/10.1021/ACSSUSCHEMENG.0C05706.
28. Lee, J.Y.; Kim, K.J. MEG Effects on Hydrolysis of Polyamide 66/Glass Fiber Composites and Mechanical Property Changes. *Molecules* **2019**, *24*, 755. https://doi.org/10.3390/MOLECULES24040755.
29. Sang, L.; Wang, C.; Wang, Y.; Hou, W. Effects of hydrothermal aging on moisture absorption and property prediction of short carbon fiber reinforced polyamide 6 composites. *Compos. Part B Eng.* **2018**, *153*, 306–314. https://doi.org/10.1016/j.compositesb.2018.08.138.
30. Li, R.; Ye, L.; Li, G. Long-Term Hydrothermal Aging Behavior and Aging Mechanism of Glass Fibre Reinforced Polyamide 6 Composites. *J. Macromol. Sci. Part B* **2018**, *57*, 67–82. https://doi.org/10.1080/00222348.2018.1432174.
31. Ksouri, I.; Haddar, N. Long term ageing of polyamide 6 and polyamide 6 reinforced with 30% of glass fibers: Temperature effect. *J. Polym. Res.* **2018**, *25*, 153. https://doi.org/10.1007/S10965-018-1551-1.
32. Geretschläger, K.J.; Wallner, G. Aging characteristics of glass fiber-reinforced polyamide in hot water and air. *Polym. Compos.* **2018**, *39*, 997–1005. https://doi.org/10.1002/PC.24070.
33. Wang, W.; Meng, L.; Leng, K.; Huang, Y. Hydrolysis of waste monomer casting nylon catalyzed by solid acids. *Polym. Degrad. Stab.* **2017**, *136*, 112–120. https://doi.org/10.1016/j.polymdegradstab.2016.12.017.
34. Ksouri, I.; De Almeida, O.; Haddar, N. Long term ageing of polyamide 6 and polyamide 6 reinforced with 30% of glass fibers: Physicochemical, mechanical and morphological characterization. *J. Polym. Res.* **2017**, *24*, 133. https://doi.org/10.1007/S10965-017-1292-6.
35. Arash, B.; Thijsse, B.J.; Pecenko, A.; Simone, A. Effect of water content on the thermal degradation of amorphous polyamide 6,6: A collective variable-driven hyperdynamics study. *Polym. Degrad. Stab.* **2017**, *146*, 260–266. https://doi.org/10.1016/j.polymdegradstab.2017.10.019.
36. Gao, L.; Ye, L.; Li, G. Long-Term Hydrothermal Aging Behavior and Life-Time Prediction of Polyamide 6. *J. Macromol. Sci. Part B* **2015**, *54*, 239–252. https://doi.org/10.1080/00222348.2014.1001660.
37. Cruz, C.; Belmonte, E.; Lux, A.; Monte, M.D.; Quaresimin, M. Multi-scale analysis of the ageing of a reinforced polyamide 66 in ethanol-based fuels. In Proceedings of the 20th International Conference on Composite Materials, Copenhagen, Denmark, 19–24 July 2015.
38. Wang, W.; Meng, L.; Huang, Y. Hydrolytic degradation of monomer casting nylon in subcritical water. *Polym. Degrad. Stab.* **2014**, *110*, 312–317. https://doi.org/10.1016/J.POLYMDEGRADSTAB.2014.09.014.

39. Haddar, N.; Ksouri, I.; Kallel, T.; Mnif, N. Effect of hygrothermal ageing on the monotonic and cyclic loading of glass fiber reinforced polyamide. *Polym. Compos.* **2014**, *35*, 501–508. https://doi.org/10.1002/pc.22688.
40. Launay, A.; Marco, Y.; Maitournam, H.; Raoult, I. Modelling the influence of temperature and relative humidity on the time-dependent mechanical behaviour of a short glass fibre reinforced polyamide. *Mech. Mater.* **2013**, *56*, 1–10. https://doi.org/10.1016/J.MECHMAT.2012.08.008.
41. Thomason, J.; Ali, J.; Anderson, J. The thermo-mechanical performance of glass-fibre reinforced polyamide 66 during glycol–water hydrolysis conditioning. *Compos. Part Appl. Sci. Manuf.* **2010**, *41*, 820–826. https://doi.org/10.1016/j.compositesa.2010.02.006.
42. Chen, J.; Liu, G.; Jin, L.; Ni, P.; Li, Z.; He, H.; Xu, Y.; Zhang, J.; Dong, J. Catalytic hydrolysis of waste nylon 6 to produce ϵ-caprolactam in sub-critical water. *J. Anal. Appl. Pyrolysis* **2010**, *87*, 50–55. https://doi.org/10.1016/J.JAAP.2009.10.004.
43. Bernstein, R.; Gillen, K.T. Nylon 6.6 accelerating aging studies: II. Long-term thermal-oxidative and hydrolysis results. *Polym. Degrad. Stab.* **2010**, *95*, 1471–1479. https://doi.org/10.1016/J.POLYMDEGRADSTAB.2010.06.018.
44. Cribbs, D.; Ogale, A. Hydrolytic Degradation of Nylon 66 Pile Carpet Fibers. *Text. Res. J.* **2003**, *95*, 1471–1479. https://doi.org/10.1177/004051750307300202.
45. Ishak, Z.A.M.; Berry, J.P. Hygrothermal aging studies of short carbon fiber reinforced nylon 6.6. *J. Appl. Polym. Sci.* **1994**, *51*, 2145–2155. https://doi.org/10.1002/APP.1994.070511306.
46. Hunt, D.G.; Darlington, M.W. Creep of nylon-6,6 during concurrent moisture changes. *Polymer* **1980**, *21*, 502–508. https://doi.org/10.1016/0032-3861(80)90215-3.
47. Gac, P.Y.L.; Fayolle, B. Impact of fillers (short glass fibers and rubber) on the hydrolysis-induced embrittlement of polyamide 6.6. *Compos. Part B-Eng.* **2018**, *153*, 256–263. https://doi.org/10.1016/J.COMPOSITESB.2018.07.028.
48. Deshoulles, Q.; Le Gall, M.; Dreanno, C.; Arhant, M.; Priour, D.; Le Gac, P. Chemical coupling between oxidation and hydrolysis in polyamide 6-A key aspect in the understanding of microplastic formation. *Polym. Degrad. Stab.* **2022**, *197*, 109851. https://doi.org/10.1016/j.polymdegradstab.2022.109851.
49. Darzi, R.; Dubowski, Y.; Posmanik, R. Hydrothermal processing of polyethylene-terephthalate and nylon-6 mixture as a plastic waste upcycling treatment: A comprehensive multi-phase analysis. *Waste Manag.* **2022**, *143*, 223–231. https://doi.org/10.1016/j.wasman.2022.03.002.
50. Da Cruz, B.d.S.M.; Tienne, L.G.P.; Gondim, F.F.; Candido, L.d.S.; Chaves, E.G.; Marques, M.d.F.V.; da Luz, F.S.; Monteiro, S.N. Graphene nanoplatelets reinforced Polyamide-11 nanocomposites thermal stability and aging for application in flexible pipelines. *J. Mater. Res. Technol.* **2022**, *18*, 1842–1854. https://doi.org/10.1016/j.jmrt.2022.03.075.
51. Costa, D.R.; Costa, M.F.; Grytten, F. Morphological changes of polyamide 11 through the corrected inherent viscosity plateau. *J. Appl. Polym. Sci.* **2022**, *139*, 52223. https://doi.org/10.1002/app.52223.
52. Arhant, M.; Lolive, E.; Bonnemains, T.; Davies, P. A study of pure hydrolysis of carbon fibre reinforced polyamide 6 composites tested under mode I loading. *Compos. Part A Appl. Sci. Manuf.* **2021**, *152*, 106719. https://doi.org/10.1016/j.compositesa.2021.106719.
53. Arhant, M.; Lolive, E.; Bonnemains, T.; Davies, P. Effect of aging on the fatigue crack growth properties of carbon-polyamide 6 thermoplastic composites using the multi ΔG-control method. *Compos. Part A Appl. Sci. Manuf.* **2022**, *161*, 107105. https://doi.org/10.1016/j.compositesa.2022.107105.
54. Olufsen, S.N.; Nygård, P.; Teixeira Pais, C.I.; Perillo, G.; Hopperstad, O.S.; Clausen, A.H. Influence of loading conditions on the tensile response of degraded polyamide 11. *Polymer* **2021**, *229*, 123966. https://doi.org/10.1016/j.polymer.2021.123966.
55. Deshoulles, Q.; Gall, M.M.L.; Dreanno, C.; Arhant, M.; Stoclet, G.; Priour, D.; Gac, P.L. Origin of embrittlement in Polyamide 6 induced by chemical degradations: Mechanisms and governing factors. *Polym. Degrad. Stab.* **2021**, *191*, 109657. https://doi.org/10.1016/J.POLYMDEGRADSTAB.2021.109657.
56. Deshoulles, Q.; Gall, M.M.L.; Dreanno, C.; Arhant, M.; Priour, D.; Gac, P.Y.L. Modelling pure polyamide 6 hydrolysis: Influence of water content in the amorphous phase. *Polym. Degrad. Stab.* **2021**, *183*, 109435. https://doi.org/10.1016/J.POLYMDEGRADSTAB.2020.109435.
57. Maïza, S.; Lefebvre, X.; Brusselle-Dupend, N.; Klopffer, M.H.; Cangémi, L.; Castagnet, S.; Grandidier, J.C. Physicochemical and mechanical degradation of polyamide 11 induced by hydrolysis and thermal aging. *J. Appl. Polym. Sci.* **2019**, *136*, 47628. https://doi.org/10.1002/app.47628.
58. Hocker, S.J.; Kim, W.T.; Schniepp, H.C.; Kranbuehl, D.E. Polymer crystallinity and the ductile to brittle transition. *Polymer* **2018**, *158*, 72–76. https://doi.org/10.1016/j.polymer.2018.10.031.
59. Hocker, S.J.; Hudson-Smith, N.V.; Smith, P.T.; Komatsu, C.H.; Dickinson, L.R.; Schniepp, H.C.; Kranbuehl, D.E. Graphene oxide reduces the hydrolytic degradation in polyamide-11. *Polymer* **2017**, *126*, 248–258. https://doi.org/10.1016/j.polymer.2017.08.034.
60. Mazan, T.; Berggren, R.; Jørgensen, J.K.; Echtermeyer, A. Aging of polyamide 11. Part 1: Evaluating degradation by thermal, mechanical, and viscometric analysis. *J. Appl. Polym. Sci.* **2015**, *132*, 41971 https://doi.org/10.1002/app.41971.
61. Hocker, S.; Rhudy, A.K.; Ginsburg, G.; Kranbuehl, D.E. Polyamide hydrolysis accelerated by small weak organic acids. *Polymer* **2014**, *55*, 5057–5064. https://doi.org/10.1016/J.POLYMER.2014.08.010.
62. Domingos, E.; Pereira, T.; Filgueiras, P.; Bueno, M.; Castro, E.R.; Guimarães, R.; Sena, G.L.; Rocha, W.F.; Romão, W. Monitoring the polyamide 11 degradation by thermal properties and X-ray fluorescence spectrometry allied to chemometric methods. *X-ray Spectrom.* **2013**,*42*, 79–86. https://doi.org/10.1002/XRS.2436.

63. Bergeret, A.; Ferry, L.; Ienny, P. Influence of the fibre/matrix interface on ageing mechanisms of glass fibre reinforced thermoplastic composites (PA-6,6, PET, PBT) in a hygrothermal environment. *Polym. Degrad. Stab.* **2009**, *94*, 1315–1324. https://doi.org/10.1016/J.POLYMDEGRADSTAB.2009.04.009.
64. Iwaya, T.; Sasaki, M.; Goto, M. Kinetic analysis for hydrothermal depolymerization of nylon 6. *Polym. Degrad. Stab.* **2006**, *91*, 1989–1995. https://doi.org/10.1016/j.polymdegradstab.2006.02.009.
65. Bernstein, R.; Derzon, D.K.; Gillen, K.T. Nylon 6.6 accelerated aging studies: Thermal–oxidative degradation and its interaction with hydrolysis. *Polym. Degrad. Stab.* **2005**, *88*, 480–488. https://doi.org/10.1016/J.POLYMDEGRADSTAB.2004.11.020.
66. Merdas, I.; Thominette, F.; Verdu, J. Hydrolytic ageing of polyamide 11—effect of carbon dioxide on polyamide 11 hydrolysis. *Polym. Degrad. Stab.* **2003**, *79*, 419–425. https://doi.org/10.1016/S0141-3910(02)00358-0.
67. Alam, T.M. Solution 17O NMR study of thermal hydrolysis in nylon 6,6. *Polymer* **2003**, *44*, 6531–6536. https://doi.org/10.1016/J.POLYMER.2003.08.003.
68. Meyer, A.; Jones, N.; Lin, Y.; Kranbuehl, D.E. Characterizing and Modeling the Hydrolysis of Polyamide-11 in a pH 7 Water Environment. *Macromolecules* **2002**, *44*, 6531–6536. https://doi.org/10.1021/MA010541O.
69. Jacques, B.; Werth, M.; Merdas, I.; Thominette, F.; Verdu, J. Hydrolytic ageing of polyamide 11. 1. Hydrolysis kinetics in water. *Polymer* **2002**, *43*, 6439–6447. https://doi.org/10.1016/S0032-3861(02)00583-9.
70. Esmizadeh, E.; Vahidifar, A.; Shojaie, S.; Naderi, G.; Kalaei, M.R.; Mekonnen, T.H. Tailoring the properties of PA6 into high-performance thermoplastic elastomer: Simultaneous reinforcement and impact property modification. *Mater. Today Commun.* **2021**, *26*, 102027. https://doi.org/https://doi.org/10.1016/j.mtcomm.2021.102027.
71. Latko-Durałek, P.; Kolbuk, D.; Kozera, R.; Boczkowska, A. Microstructural Characterization and Mechanical Properties of PA11 Nanocomposite Fibers. *J. Mater. Eng. Perform.* **2015**, *25*, 68–75. https://doi.org/10.1007/s11665-015-1817-2.
72. Chaupart, N.; Serpe, G.; Verdu, J. Molecular weight distribution and mass changes during polyamide hydrolysis. *Polymer* **1998**, *39*, 1375–1380 https://doi.org/10.1016/S0032-3861(97)00414-X.
73. Abastari; Sakai, T.; Sembokuya, H.; Kubouchi, M.; Tsuda, K. Study on permeation behavior and chemical degradation of PA66 in acid solution. *Polym. Degrad. Stab.* **2007**, *39*, 1375–1380. https://doi.org/10.1016/J.POLYMDEGRADSTAB.2006.12.002.
74. Liang, J.; Xu, Y.; Wei, Z.; Song, P.; Chen, G.; Zhang, W. Mechanical properties, crystallization and melting behaviors of carbon fiber-reinforced PA6 composites. *J. Therm. Anal. Calorim.* **2014**, *115*, 209–218. https://doi.org/10.1007/s10973-013-3184-2.
75. Gianchandani, J.; Spruiell, J.E.; Clark, E.S. Polymorphism and orientation development in melt spinning, drawing, and annealing of nylon-6 filaments. *J. Appl. Polym. Sci.* **1982**, *27*, 3527–3551. https://doi.org/10.1002/app.1982.070270928.
76. Li, L.; Li, C.Y.; Ni, C.; Rong, L.; Hsiao, B. Structure and crystallization behavior of Nylon 66/multi-walled carbon nanotube nanocomposites at low carbon nanotube contents. *Polymer* **2007**, *48*, 3452–3460. https://doi.org/10.1016/j.polymer.2007.04.030.
77. Gurato, G.; Fichera, A.; Grandi, F.Z.; Zannetti, R.; Canal, P. Crystallinity and polymorphism of 6-polyamide. *Die Makromol. Chem.* **1974**, *175*, 953–975. https://doi.org/https://doi.org/10.1002/macp.1974.021750322.
78. Inoue, M. Studies on crystallization of high polymers by differential thermal analysis. *J. Polym. Sci. Part A Gen. Pap.* **1963**, *1*, 2697–2709. https://doi.org/10.1002/pol.1963.100010813.
79. Panaitescu, D.M.; Frone, A.N.; Nicolae, C. Micro- and nano-mechanical characterization of polyamide 11 and its composites containing cellulose nanofibers. *Eur. Polym. J.* **2013**, *49*, 3857–3866. https://doi.org/10.1016/j.eurpolymj.2013.09.031.
80. Roguet, E.; Tencé-Girault, S.; Castagnet, S.; Grandidier, J.; Hochstetter, G. Micromechanisms involved in the atypical tensile behavior observed in polyamide 11 at high temperature. *J. Polym. Sci. Part Polym. Phys.* **2007**, *45*, 3046–3059, https://doi.org/https://doi.org/10.1002/polb.21299.
81. Pepin, J.; Miri, V.; Lefebvre, J.M. New Insights into the Brill Transition in Polyamide 11 and Polyamide 6. *Macromolecules* **2016**, *49*, 564–573, https://doi.org/10.1021/acs.macromol.5b01701.
82. Zhang, Q.; Mo, Z.; Liu, S.; Zhang, H. Influence of Annealing on Structure of Nylon 11. *Macromolecules* **2000**, *33*, 5999–6005. https://doi.org/10.1021/ma000298d.
83. Ram, F.; Radhakrishnan, S.; Ambone, T.; Shanmuganathan, K. Highly Flexible Mechanical Energy Harvester Based on Nylon 11 Ferroelectric Nanocomposites. *ACS Appl. Polym. Mater.* **2019**, *1*, 1998–2005. https://doi.org/10.1021/acsapm.9b00246.
84. Dhanalakshmi, M.; Jog, J.P. Preparation and characterization of electrospun fibers of Nylon 11. *Express Polym. Lett.* **2008**, *2*, 540–545. https://doi.org/10.3144/expresspolymlett.2008.65.
85. Fernandez, J.O.; Swallowe, G.M.; Lee, S.F. Crystallization of Nylon 11 under compressive high strain rates. *J. Appl. Polym. Sci.* **2001**, *80*, 2031–2038. https://doi.org/10.1002/app.1301.
86. Benobeidallah, B.; Benhamida, A.; Dorigato, A.; Sola, A.; Messori, M.; Pegoretti, A. Structure and Properties of Polyamide 11 Nanocomposites Filled with Fibrous Palygorskite Clay. *J. Renew. Mater.* **2019**, *7*, 89–102. https://doi.org/10.32604/jrm.2019.00136.
87. Mago, G.; Kalyon, D.M.; Fisher, F.T. Nanocomposites of polyamide-11 and carbon nanostructures: Development of microstructure and ultimate properties following solution processing. *J. Polym. Sci. Part B Polym. Phys.* **2011**, *49*, 1311–1321. https://doi.org/https://doi.org/10.1002/polb.22311.
88. Romão, W.; Franco, M.F.; Corilo, Y.E.; Eberlin, M.N.; Spinacé, M.A.; De Paoli, M.A. Poly (ethylene terephthalate) thermo-mechanical and thermo-oxidative degradation mechanisms. *Polym. Degrad. Stab.* **2009**, *94*, 1849–1859. https://doi.org/10.1016/j.polymdegradstab.2009.05.017.

89. Romão, W.; Franco, M.F.; Bueno, M.I.M.; De Paoli, M.A. Distinguishing between virgin and post-consumption bottle-grade poly (ethylene terephthalate) using thermal properties. *Polym. Test.* **2010**, *29*, 879–885. https://doi.org/10.1016/j.polymertesting.2010.05.009.
90. Wypych, G. 3-Mechanisms of UV Stabilization. In *Handbook of UV Degradation and Stabilization*, 2nd ed.; ChemTec Publishing: Toronto, ON, Canada, 2015; pp. 37–65. https://doi.org/10.1016/B978-1-895198-86-7.50005-X.
91. Socrates, G. *Infrared and Raman Characteristic Group Frequencies: Tables and Charts*, 3rd ed.; Wiley: Hoboken, NJ, USA, 2001.
92. Skrovanek, D.J.; Painter, P.C.; Coleman, M.M. Hydrogen bonding in polymers. 2. Infrared temperature studies of nylon 11. *Macromolecules* **1986**, *19*, 699–705. https://doi.org/10.1021/ma00157a037.
93. Mazan, T.; Jørgensen, J.K.; Echtermeyer, A. Aging of polyamide 11. Part 2: General multiscale model of the hydrolytic degradation applied to predict the morphology evolution. *J. Appl. Polym. Sci.* **2015**, *132*, 42630. https://doi.org/10.1002/app.42630.
94. Mazan, T.; Jørgensen, J.K.; Echtermeyer, A. Aging of polyamide 11. Part 3: Multiscale model predicting the mechanical properties after hydrolytic degradation. *J. Appl. Polym. Sci.* **2015**, *132*, 42792. https://doi.org/10.1002/app.42792.
95. Andrady, A.L. The plastic in microplastics: A review. *Mar. Pollut. Bull.* **2017**, *119*, 12–22. https://doi.org/10.1016/j.marpolbul.2017.01.082.
96. Greco, R.; Ragosta, G. Isotactic polypropylenes of different molecular characteristics: Influence of crystallization conditions and annealing on the fracture behaviour. *J. Mater. Sci.* **1988**, *23*, 4171–4180. https://doi.org/10.1007/BF01106853.
97. Bessell, T.J.; Hull, D.; Shortall, J.B. The effect of polymerization conditions and crystallinity on the mechanical properties and fracture of spherulitic nylon 6. *J. Mater. Sci.* **1975**, *10*, 1127–1136. https://doi.org/10.1007/BF00541393.
98. Fornes, T.; Yoon, P.; Keskkula, H.; Paul, D. Nylon 6 nanocomposites: The effect of matrix molecular weight. *Polymer* **2001**, *42*, 09929–09940. https://doi.org/10.1016/S0032-3861(01)00552-3.
99. Steeman, P.; Nijenhuis, A. The effect of random branching on the balance between flow and mechanical properties of polyamide-6. *Polymer* **2010**, *51*, 2700–2707. https://doi.org/10.1016/j.polymer.2010.04.017.
100. Millot, C.; Séguéla, R.; Lame, O.; Fillot, L.A.; Rochas, C.; Sotta, P. Tensile Deformation of Bulk Polyamide 6 in the Preyield Strain Range. Micro–Macro Strain Relationships via in Situ SAXS and WAXS. *Macromolecules* **2017**, *50*, 1541–1553. https://doi.org/10.1021/acs.macromol.6b02471.
101. Huang, Y.L.; Brown, N. Dependence of slow crack growth in polyethylene on butyl branch density: Morphology and theory. *J. Polym. Sci. Part B Polym. Phys.* **1991**, *29*, 129–137. https://doi.org/10.1002/polb.1991.090290116.
102. Seguela, R. Critical review of the molecular topology of semicrystalline polymers: The origin and assessment of intercrystalline tie molecules and chain entanglements. *J. Polym. Sci. Part B Polym. Phys.* **2005**, *43*, 1729–1748. https://doi.org/10.1002/polb.20414.
103. Arhant, M.; Gall, M.L.; Gac, P.Y.L.; Davies, P. Impact of hydrolytic degradation on mechanical properties of PET-Towards an understanding of microplastics formation. *Polym. Degrad. Stab.* **2019**, *161*, 175–182. https://doi.org/10.1016/J.POLYMDEGRADSTAB.2019.01.021.